Seasonal Mg isotopic variation in the middle Yellow River: Sources and fractionation

Long-Fei Gou[1,2], Zhangdong Jin[2,1*], Albert Galy[3], Yang Xu[2], Jun Xiao[2,1], Yibo Yang[4], Julien Bouchez[5], Philip A. E. Pogge von Strandmann[6], Chenyang Jin[5,7], Shouye Yang[7], Zhi-Qi Zhao[8]

1 Department of Geography, Chang'an University, 710054, China;

2 State Key Laboratory of Loess and Quaternary Geology, Institute of Earth Environment, Chinese Academy of Sciences, Xi'an 710061, China;

3 Centre de Recherches Pétrographiques et Géochimiques, UMR7358, CNRS, Université de Lorraine, 54500 Vandoeuvre les Nancy, France;

4 Key Laboratory of Continental Collision and Plateau Uplift, Institute of Tibetan Plateau Research, Chinese Academy of Sciences, Beijing 100101, China;

5 Institut de Physique du Globe de Paris, Université Paris Diderot, Sorbonne Paris Cité, CNRS, UMR 7154, 1 rue Jussieu, 75238 Paris, France;

6 Institute of Geosciences, Johannes Gutenberg-Universitat Mainz, 55128 Mainz, Germany;

7 Department of Marine Geology, Tongji University, Shanghai 200092, China.

8 School of Earth Sciences and Resources, Chang'an University, 710054, China.

Corresponding author: Zhangdong Jin (zhdjin@ieecas.cn)

Abstract: In order to better understand how stable metal isotope signals in large rivers can be used to constrain present and past weathering, the seasonal riverine Mg-Sr isotopic pattern in the middle Yellow River was systematically investigated based upon weekly collected samples for the whole year of 2013. The results demonstrate that Mg is mainly transported in the dissolved form (65%) in this river system and that 45% of the total dissolved Mg is transported during the monsoon seasons, with 2% exported over 4 days (~1% annual time) during a single storm event. Dissolved Mg in the middle Yellow River is dominantly derived from both silicate and carbonate (82-89%) in this arid to semi-arid region, with limited evaporite contribution (~7%). Lithological mixing is the first order control on riverine dissolved Mg and Sr isotopes, with a contribution from ~40% carbonate dissolution and ~60% from silicate dissolution in the dry seasons, and ~50% carbonate and ~50% silicate during the monsoon seasons according to δ^{26}Mg signals. Furthermore, a significant role of prior calcite precipitation (PCP) can be quantified, which fractionates Mg isotopes by about 0.17‰ to 0.39‰ positively depending on the choice of elemental and isotope partition of Mg in secondary carbonates. Clay formation following PCP further fractionates riverine Mg isotopes to the negative side. An ~0.2‰ decrease of riverine Mg isotopes is attributable to (1) a single storm event causing carbonate dissolution and (2) delayed delivery of depleted waters to rivers (~3 months after the storm event) because of subsurface hydrological circulation. Annually, the weighted average riverine δ^{26}Mg (-1.05‰) in the middle Yellow River is identical to the global average (-1.09‰). Despite the significant impact of lithology on the riverine dissolved

Mg isotope signature, the mixing proportions of different Mg sources remain virtually constant, even when there are huge contrast of temperature, hydrology, and precipitation seasonally along the year, providing a basis for dissolved δ^{26}Mg response to climatic forcing on the continental scale. This means that significant changes in the sedimentary Mg isotope records would reflect extreme conditions in deep time.

Key words: Mg isotopes; Isotopic fractionation; Seasonal variation; Sr isotopes; Prior calcite precipitation (PCP); Chemical weathering; Storm event; The Yellow River; Chinese Loess Plateau (CLP)

1. Introduction

Chemical weathering is one of the most important geochemical processes on the Earth's surface, leading to the production of water-bearing minerals and thus to hydration of the continental crust, and regulating global climate by sequestering atmospheric CO_2 on geological time-scales (e.g., Walker et al., 1981; Berner et al., 1983; Hilton and West, 2020). However, the role of CO_2 removal by chemical weathering is still debated, given the numerous factors acting on chemical weathering (e.g., Gaillardet et al., 1999; West et al., 2005; Hilton and West, 2020). Isotopic proxies (e.g., Sr, Li, Si, Ca, and Mg, etc.) have the potential to enhance our understanding of the processes and dynamics of chemical weathering (e.g., Palmer and Edmond, 1992; Huh et al., 1998; Georg et al., 2007; Tipper et al., 2006b; Teng, 2017).

Magnesium (Mg) and calcium (Ca) are the two major base cations present in silicate minerals that combine with atmospheric CO_2 leading to carbon sequestration into carbonates (Walker et al., 1981; Berner et al., 1983; Gaillardet et al., 1999). Mg is a major element in both silicates and carbonates, but both reservoirs have distinct Mg isotope ratios (expressed as δ^{26}Mg), with a relatively homogeneous δ^{26}Mg value of major igneous rocks (i.e., +0.1‰ to -0.6‰, average -0.22‰, Li et al., 2010; Teng, 2017), while a hetegeneous negative Mg isotopes of carbonates (i.e., < -0.80‰, Fig. S1). Seawater shows a mean δ^{26}Mg value of -0.83‰ (Fig. S1). Hence, Mg isotopes in rivers are potentially a sensitive tracer to evaluate the relative roles of carbonate and silicate weathering, biological Mg cycle, and associated C-sequestration. However, the dominant controls on riverine Mg isotopes ratios are still debated, including the following control factors or processes:

(1) Preferential incorporation of either light or heavy Mg isotopes during formation of secondary clay minerals (Tipper et al., 2006b, 2006c; Pogge von Strandmann et al., 2008a; Immenhauser et al., 2010; Opfergelt et al., 2012; Riechelmann et al., 2012b; Ryu et al., 2016; Zhang et al., 2018; Hindshaw et al., 2020) and of light Mg isotopes during carbonate precipitation (Galy et al., 2002; Tipper et al., 2006c; Buhl et al., 2007; Immenhauser et al., 2010; Li et al., 2012; Riechelmann et al., 2012b; Pogge von Strandmann, et al., 2019, 2020).

(2) Preferential adsorption and desorption of heavy Mg isotopes on secondary oxides, hydroxides, and clay minerals (Huang et al., 2012; Pogge von Strandmann et al., 2012; Tipper et al., 2012a; Fan et al., 2016).

(3) Mg isotopic fractionation during the early stages of weathering by organic or inorganic processes (Wimpenny et al., 2010; Balland-Boulo-Bi et al., 2019).

(4) Mixing of waters carrying Mg released of solutions stemming from the congruent dissolution of minerals with distinct Mg isotope composition (Pogge von Strandmann et al., 2008a, 2020; Wimpenny et al., 2011; Lee et al., 2014; Ryu et al., 2016; Li et al., 2020).

In turn, the above-listed factors and/or processes responsible for Mg isotope fractionation may (Wimpenny et al., 2014; Ma et al., 2019) or may not (Tipper et al., 2006c) be sensitive to climate. In fact, due to the poor understanding of the large-scale controls on Mg isotope fractionation, it is not yet known how global riverine Mg isotopes respond to climate shift, although such an understanding is required for the robust interpretation of Mg isotope records in sedimentary archives, be it in marine documents (Kasemann et al., 2014; Pogge von Strandmann et al., 2014; Higgins and Schrag, 2015; He et al., 2020), loess-paleosol sequences (Wimpenny et al., 2014; Ma et al., 2019), or speleothems (Galy et al., 2002; Buhl et al., 2007; Immenhauser et al., 2010; Riechelmann et al., 2012a, b).

To better constrain the effect of climate on river chemistry, time series of river water samples collected under different meteorological settings is always helpful (e.g., Galy and France-Lanord, 1999; Tipper et al., 2006a; Jin et al., 2011; Zhang et al., 2015; Gou et al., 2019b, 2020). Indeed, within such time series, tectonics and lithology are held relative constant, while the temporal variations of temperature, discharge, and precipitation are known. Seasonal variations in δ^{26}Mg in small catchments (~100 km^2) have been shown to be significant (Pogge von Strandmann et al., 2020). However, seasonal variations of Mg isotopes in large catchments appear limited (Tipper et al., 2012b; Hindshaw et al., 2019; Mavromatis et al., 2020), so that poor understanding of seasonal Mg isotope variation on global scale hampers its further applications in deep time.

In this study, we investigated how riverine δ^{26}Mg shifts seasonally in the middle reaches of the Yellow River, based on a weekly water sampling scheme covering a full hydrological year. The middle Yellow River drains easily erodible, homogeneous loess on the Chinese Loess Plateau (CLP) that is representative to the average chemical compositions of the upper continental crust (UCC, Taylor et al., 1983) and is subjected to pronounced seasonal temperature, precipitation, and discharge swings due to the East Asian summer monsoon and the Westerly jet, making it one of the most suitable settings to define the response of riverine Mg isotopes to changes in temperature, precipitation, and discharge on the continental scale. In addition, due to the easy erodible of loess, the SPM in the middle Yellow River is actually loess mainly derived from the CLP (Li et al., 1984; Fan et al., 2016; Gou et al., 2019, 2020). We found that in such (semi-)arid regions, significant changes in climate parameters play a limited direct role on Mg isotopic variation (~0.2‰). We then addressed this limited variation as a combined result of prior calcite precipitation (PCP), clay formation, and seasonality in hydrology, providing a case study of how dissolved δ^{26}Mg values response to climatic forcing on the continental scale.

2 Study area

2.1 Geography

The Yellow River originates from the northeastern Tibetan Plateau with an elevation of over 4000 m, drains across the CLP at its middle reaches, and discharges into the Bohai Sea (Fig. 1; Zhang et al., 1995; Wu et al., 2005). It is the fifth longest (5464 km) and the most sediment-laden river in the world with 10.8×10^8 t/yr of sediment discharge (Zhang et al., 1995). Because of the high erodibility of loess, the CLP is the largest sediment source to the Yellow River between Hekou town (Toudaoguai) and Tongguan, contributing nearly 90% sediment (Wang et al., 2010; Yu et al., 2013, Fig. 1), although only ~40% of water is sourced from the 21 tributaries with a catchment area larger than 1000 km^2 that all drain the CLP (Zhang et al., 2015, Fig. 1). By contrast, the upper reaches contribute ~60% of annual water discharge (Q_w, 25 km^3/yr), but merely ~10% of annual sediment load (Li et al., 2018).

2.2 Geology

The Yellow River drains the old Sino-Korean Shield formed during the Archaean to Proterozoic Eras (Zhang et al., 1995), featuring rock outcrops dating from the Precambrian to the Quaternary. In the upper river basin above Lanzhou, at an elevation above 2000 m, rocks are mainly composed of limestone, low-grade metamorphic rocks and clastic sediments interlaced with volcanic rocks and evaporites (Chen et al., 2005). The middle Yellow River drains through the CLP, covered by Quaternary eolian loess and loess-like deposits, which account for 44% of the total catchment area (Fig. 1). Loess is homogeneous, porous, friable, pale yellow, slightly coherent, typically non-stratified and often calcareous (Liu, 1988), and has variable δ^{26}Mg values (-0.32‰ to +0.05‰ (Li et al., 2010); -0.79‰ to -0.19‰ (Wimpenny et al., 2014)). Mineralogically, loess is composed of quartz, feldspar, calcite, mica, minor heavy minerals, and with small amounts of evaporites such as halite, gypsum, and mirabilite (Liu, 1988; Zhang et al., 1995; Yokoo et al., 2004). Severe physical erosion on the CLP leads to the formation of numerous gullies and gives the Yellow River an extremely high sediment yield, in particular during the monsoonal seasons. As a result, suspended particle matter (SPM) in the Yellow River is of the same mineralogical and geochemical compositions as the loess of the CLP (Li et al., 1984; Zhang et al., 1995).

2.3 Climate

The Yellow River basin is characterized by a temperate climate. Regions of the upper reaches of the Yellow River basin are cold-arid to semi-arid with an annual mean temperature ranging from 1°C to 8°C, whereas the regions of the middle reaches are semi-arid to semi-humid with annual mean temperatures ranging from 8°C to 14°C (Chen et al., 2005). Despite the fact that the mean annual precipitation is quite variable across the river basin, increasing from 368 mm in the upper reaches to 530 mm in the middle reaches

(Wang et al., 2007), owing to the Asian summer monsoon, the seasonal climate variation is more pronounced than the spatial one. Rainfall is negligible in winter, but it is high, with frequent rainstorms, in summer, especially in the middle reaches of the Yellow River. The rainy season (between June and mid-September) accounts for 80% of the annual precipitation (500-600 mm, Zhang et al., 1995). Note that there was a single storm event (22nd to 25th July), accounting for ~6% precipitation in 2013 (Gou et al., 2019b).

3 Sampling and methodology

3.1 Sampling protocol

3.1.1 Field sampling

A total of 60 river water samples were collected weekly in 2013 at the Longmen hydrological station (N 35°40′06.43″, E 110°35′22.88″). This station is located in the middle Yellow River where waters from most tributaries draining the CLP are already mixed, but its drainage basin excludes the drainage basins of the Fen and Wei Rivers that host highly populated areas (Fig. 1). Four samples (Nos. LM13-31 to 13-34) were collected daily during the storm event (Zhang et al., 2015; Gou et al., 2019b, 2020), and three rain samples were collected in July and August 2013 to appraise atmospheric inputs. A sewage sample (TKT1) was collected in a farmland adjacent to the station to constrain the composition of anthropogenic input (Gou et al., 2019b, 2020).

All river water samples were collected 0.5 m below the surface in the middle of the river channel. For each sample, water temperature, pH, electrical conductivity (EC) were measured *in situ* by a multi-meter (Hanna® Instruments, Model: H198129). All water samples were filtered on site through 0.2-μm porosity nylon filters. Filtered water samples were stored in pre-cleaned polyethylene bottles, acidified to pH<2 with distilled HNO_3 and stored at 4°C before major cation concentrations, strontium and magnesium isotope analyses. Another non-acidified 30 mL bottle treated with the same way for anion analyses.

3.1.2 Sequential extraction of loess material

Five fresh loess samples were collected from 5 typical layers (L1, S1, S5, L9, and the red clay) of a loess profile at Lingtai and underwent sequential extraction for Mg isotopes (Tessier et al., 1979; Yokoo et al., 2004; Gou et al., 2019b, 2020). Briefly, 0.5 g of ground loess was leached with 10 mL 18.2 MΩ cm water for 5 minutes, centrifuged and filtered to collect the water-soluble fraction, referred to as the "evaporite" fraction below; the residue was then leached for 2 h with 10 mL 5% acetic acid (HAc) solution at 25ºC and then centrifuged to collect the "carbonate" fraction of loess (Tessier et al., 1979; Yokoo et al., 2004), which may also involves minor iron oxides. The residues of the leaching procedures were digested with 10 mL HF–HCl–HNO_3 (Yokoo et al., 2004; An et al., 2014; Gou et al., 2019a) to constrain the "silicate" fraction of loess.

3.2. Analyses

Concentrations of major ions for all river samples were reported by Zhang et al. (2015). Major cations of extracted samples were determined by a Leeman Labs Profile inductively coupled plasma atomic emission spectroscopy (ICP-AES) instrument, with a RSD (relative standard deviation) better than 5% reproducibility according to replicates and references materials.

3.2.1 $^{87}Sr/^{86}Sr$ ratio analyses

For Sr separation, sample solutions containing ~400 ng Sr were evaporated to dryness in pre-cleaned beakers and then re-dissolved in 1 mL 3 M HNO_3. Strontium was then purified from matrix using the Micro Spec resin (Sr-SPEC) with 3 mL Milli-Q H_2O (e.g., Jin et al., 2011). Strontium isotope ratios ($^{87}Sr/^{86}Sr$) were measured using a Thermo-Fisher *Neptune Plus* MC-ICP-MS. Accuracy and precision were evaluated using the NIST reference material SRM987 via internally normalized radiogenic Sr isotope compositions as $^{86}Sr/^{88}Sr$ of 0.1194, returning $^{87}Sr/^{86}Sr$ 0.710253 ± 0.000016 (2 s.d., n=15, recommended value of 0.710245, see Jin et al., (2011)), in agreement with previously reported values in our lab(e.g., Jin et al., 2011; Xu et al., 2021).

3.2.2 Mg isotope analyses

For Mg isotope analysis, ~1 mL of water sample containing ~40 μg Mg was dried down and re-dissolved in distilled concentrated HNO_3. This solution was dried again and re-dissolved in 1 mL 2 M HNO_3 for column chromatography. Sample purification was performed twice using 2 mL of a cation exchange resin (AG50W X-12, 200-400 mesh, modified from An et al. (2014)), with 2 M HNO_3+0.5 M HF and 1 M HNO_3 as the eluent. For each sample, column recovery was assessed by collecting splits before, in, and after the Mg cut, and analyzed using ICP-MS. The relative recovery was better than 99.9% (Gou et al., 2019a) for all samples and the purity of the Mg fraction (expressed as X/Mg molar ratio, X refers to individual element, Gou et al., 2019a) in all samples reported in this study was less than 0.1, leading to insignificant matrix effect on the accuracy of the measured Mg isotopic composition (Galy et al., 2001; Huang et al., 2009; An et al., 2014; Teng et al., 2015; Gou et al., 2019a). The total procedural blank of this method was less than 1.8 ng Mg, negligible relative to 40 μg of Mg analyzed in each sample

(Gou et al., 2019a).

Isotope analyses were all performed at IEE-CAS, on a *Neptune Plus* MC-ICP-MS via sample-standard-bracketing method, with ~200 ng/mL Mg. The δ^{26}Mg values are given as:

$$\delta^{26}\mathrm{Mg} = [^{26}\mathrm{Mg}/^{24}\mathrm{Mg})_{\mathrm{sample}}/(^{26}\mathrm{Mg}/^{24}\mathrm{Mg})_{\mathrm{DSM\text{-}3}}-1] \times 1000 \qquad \text{Eq (1)}$$

where DSM-3 is the standard reference material of Mg (Galy et al., 2003).

Triple measurements were conducted to calculate average and standard deviation for each sample. Two pure-Mg standards (namely Cambridge-1 and IGGCAS-Mg, respectively) were run repeatedly for a 5 years period yielding δ^{26}Mg = -2.60 ± 0.07‰ (2 s.d., n = 51) and -1.75 ± 0.07‰ (2 s.d., n = 53), respectively, in agreement with previous studies (Galy et al., 2001, 2002; Tipper et al., 2006b, c, 2008, 2010, 2012a, b; Pogge von Strandmann, 2008; Tanimizu, 2008; Bolou-Bi et al., 2009; Chakrabarti and Jacobsen, 2010; Huang et al., 2009; Bizzarro et al., 2011; Larsen et al., 2011; Wang et al., 2011; Choi et al., 2012; An et al., 2014; Dessert et al., 2015; Coath et al., 2017; Hin et al., 2017; Sikdar and Rai, 2017, Gou et al., 2019a; Xu et al., 2021). In addition, another in-house standard (IEECAS-Mg) was also run repeatedly at IEE-CAS, yielding a δ^{26}Mg of 0.30 ± 0.07‰ (2 s.d., n = 21), which is indistinguishable to that measured at the Centre de Recherches Pétrographiques et Géochimiques (CRPG, France, $\delta^{26}\mathrm{Mg}_{\mathrm{IEECAS}}$ = 0.30 ± 0.07‰, 2 s.d., n = 5).

Two rock reference materials (AGV-2, BHVO-2) and a seawater reference material (NASS-6) were purified following the above procedure yielding δ^{26}Mg = -0.19 ± 0.04‰ (2 s.d., n = 6, number of digestions = 6, number of separate column passes = 6), δ^{26}Mg = -0.22 ± 0.06‰ (2 s.d., n = 16, digestions = 16, column passes = 16), and δ^{26}Mg = -0.83 ± 0.07‰ (2 s.d., n = 13, column passes = 13), respectively, over a five-year period, in agreement with previously reported values (e.g., Pogge von Strandmann, 2008; Foster et al., 2010; An et al., 2014; Huang et al., 2015; Teng et al. 2015; Teng, 2017; Coath et al., 2017; Hin et al., 2017; Sikdar and Rai, 2017; Xu et al., 2021). Based on the long-term in-house, rock, seawater reference materials, and the replicates, the 5-year external reproducibility for δ^{26}Mg measurements is better than 0.07‰ (2 s.d.; Gou et al., 2019a).

4 Results

4.1 Hydrology and suspended sediment concentration

Over the year of 2013, the water temperature of the middle Yellow River monotonously increased from a January minimum of 0°C to an August maximum of 28.8°C, and then smoothly decreased (Figs. 2 and S2). During the monsoon seasons (June to mid-September), the daily air temperatures were generally above 20°C.

The mean Q_w gauged at the Longmen hydrological station was 25 km^3/yr in 2013. During the dry seasons, these low Q_w values were first reached in January–February, and then they peaked in March followed by a minimum of 152 m^3/s in May (Figs. 2 and S2). We define the first small Q_w peak as an “ice melting interval” because it was a result of ice melt from the 16th of March to the 13th of April when the air temperature above 0°C. During the monsoon seasons, the high Q_w reflects the frequent, monsoon-driven precipitation within the Yellow River basin. Notably, there was a storm event from the 22nd to the 25th of July, resulting in the maximum Q_w (2400 m^3/s) of the year 2013 (Zhang et al., 2015; Gou et al., 2019b, 2020).

All the waters of the middle Yellow River collected in 2013 were alkaline, with pH values between 7.05 and 8.71 (Fig. 2, Fan et al., 2016). The annual dissolved phase flux of the middle Yellow River for the year 2013 was 1.9 $\times 10^{10}$ kg/yr. Compared to the annual dissolved phase flux from the upper Yellow River (above Lanzhou, Fig. 1) of 6.1×10^9 kg/yr observed for the year 2016 (Li et al., 2018), we can estimate that the upper Yellow River supplies about 1/3 of the middle Yellow River's dissolved phase. Note that the above estimation bears uncertainty because of potential inter-annual variability, but such uncertainty appears limited according to 4 decades record of TDS at Longmen (Chen et al., 2003).

The Yellow River is well-known for being sediment-laden, contributing ~10% of the global sediment delivery to the oceans (Zhang et al., 1995; Saito et al., 2001). Seasonal variations of SPM in the middle Yellow River over the year 2013 spans five orders of magnitude (Fig. 2). SPM was low and constant during the dry seasons with a spike during the ice melting period, whereas high concentrations and fluxes of SPM were observed during the monsoon seasons (Fig. 2). The highest concentrations and fluxes of SPM were recorded during the storm event. Overall, instantaneous physical erosion rates (PER, Zhang et al., 2015) during the monsoon seasons were one to three orders of magnitude higher than those of the dry seasons (Figs. 2 and 3), resulting from intense loess erosion during the monsoon season (Zhang et al., 2015; Gou et al., 2019b, 2020).

4.2 Mg concentrations and elemental ratios

Dissolved river Mg concentrations (hereafter refers to as $[Mg]_{rw}$) and $\delta^{26}Mg_{rw}$ values of the time-series samples are shown in Fig. 2 and Table S1. Over the year of 2013, the $[Mg]_{rw}$ in the Yellow River waters were on average

1285 μmol/L, ranging from 992 μmol/L for the storm event during the monsoon season to 2024 μmol/L in winter, showing doubled Mg concentrations between the wet and dry seasons. Meanwhile, the Q_w showed a variation of one magnitude (Fig. 2), indicating a Mg retention in the basin during high discharge, even if both co-vary. The $[Mg]_{rw}$ showed its first low value when the air temperature was above zero during the early ice melting interval (Ran et al., 2015; Zhang et al., 2015; Gou et al., 2019b, 2020). After the ice melting peak, the $[Mg]_{rw}$ remained at relatively low concentrations, until the storm event where $[Mg]_{rw}$ reached the lowest value of the whole year (992 μmol/L, Zhang et al., 2015). Then the $[Mg]_{rw}$ increased again until a period of $[Mg]_{rw}$ fluctuations within relatively high values (1531-1679 μmol/L; Fig. 2). Notably, $[Mg]_{rw}$ did not return to values similar to those of the beginning of 2013 (Fig. 2). All these $[Mg]_{rw}$ values fall within the range reported elsewhere for samples of the Yellow River (663 to 26100 μmol/L**,** Fan et al., 2016).

Seasonal variations of Sr/Ca, Mg/Ca, and Sr/Mg molar ratios in the middle Yellow River over the year of 2013 were shown in Fig. S2. Generally, variations of the Sr/Ca ratio mimicked those of the Mg/Ca molar ratio, both showing a slight decrease followed by an increase to their highest values at the beginning of the monsoon season (*i.e.*, Mg/Ca from 0.70 to 0.90; Sr/Ca from 6.5 to 8.0, respectively), with a dramatic decrease in response to the storm event (Mg/Ca 0.65 and Sr/Ca 7.0, respectively), and a quick rebound to high values again after the storm event (Mg/Ca 0.85 and Sr/Ca 8.0) followed by a gradual decrease in both ratios (Mg/Ca 0.75 and Sr/Ca 6.5). The Sr/Mg ratio was rather stable before the monsoon season (~8.0), with an abrupt increase in June, eventually reaching its highest value during the storm event (~10.0). The

Sr/Mg ratio decreased with fluctuations towards the end of 2013 (~8.0), followed by an increase of Sr/Mg during in mid-November (~9.0, ~3 months after the storm event; Fig. S2).

The dissolved Mg concentrations of the rainwater samples ($[Mg]_{rain}$) were relatively homogeneous, with an average of ~45 µmol/L (Table S2; Zhang et al., 2015), higher than measured in rainwater samples elsewhere (0.9-38.4 umol/L, Tipper et al., 2006c, 2012a; Pogge von Strandmann et al., 2008; Dessert et al., 2015; Fries et al., 2019). This could be related to a higher dust contribution in the studied area, leading to the dissolution of Mg-rich particles into rain droplets (Jin et al., 2011; Fan et al., 2016; Gou et al., 2019b). The dissolved Mg concentration of the sewage water collected in a farmland near the hydrological station was 12.3 mmol/L (Table S2).

Ionic compositions of the leaching experiment of the Lingtai loess were reported in Table S3. The evaporite-fraction generally had a low Mg concentration (~0.27 ± 0.26 mg/g; in mg Mg per g of the initial bulk sample); the carbonate fraction showed an intermediate Mg concentration (~1.00 ± 0.87 mg/g); the Mg concentration in the silicate fraction was high (20.90 ± 8.54 mg/g), in line to the value of the UCC (Taylor et al., 1983; Li et al., 2010; Teng et al., 2010; Teng, 2017). Given that the SPM in the middle Yellow River shares the same chemical and mineralogical composition with CLP loess (Li et al., 1984; Fan et al., 2016; Gou et al., 2019b, 2020), a Mg concentration in SPM ($[Mg]_{SPM}$) of 22.2 ± 9.7 mg/g, as measured for loess (Table S3, Taylor et al., 1983; Yokoo et al., 2004) is used hereafter in the study.

4.3. $^{87}Sr/^{86}Sr$ ratios

In 2013, the $^{87}Sr/^{86}Sr$ values of the middle Yellow River water

($^{87}Sr/^{86}Sr_{rw}$) ranged between 0.71098 and 0.71129 (Fig. 2, Table S1). The $^{87}Sr/^{86}Sr_{rw}$ remained at relatively high values (averaging 0.71123) until the storm event where they reached their first minimum (0.71110), but rebounded to prior values within three weeks, and eventually attained a maximum (0.71099) one month after the storm event (Fig. 2). After the monsoon, $^{87}Sr/^{86}Sr_{rw}$ showed some fluctuations, followed by a dramatic drop to reach the second minimum (0.71098) in mid-November. Then $^{87}Sr/^{86}Sr_{rw}$ rebounded back to initial values (0.71123) and maintained those values for the rest of the year.

4.4 δ^{26}Mg

In 2013, the δ^{26}Mg values of the middle Yellow River water ($\delta^{26}Mg_{rw}$) ranged from -1.20‰ to -0.98‰ (Fig. 2), the long-term external reproducibility is better than 0.07‰. This range is smaller than that reported for observed relative seasonal variability in small catchments of the Himalayas or the Swiss Alps (Tipper et al. 2006b, 2012b), is much smaller when compared to spatial variability (~2.5‰) across global river systems (Tipper et al., 2006b, c; Brenot et al., 2008; Pogge von Strandmann et al., 2008a, b, 2012; Wimpenny et al., 2011; Riechelmann et al., 2012b; Lee et al., 2014; Dessert et al., 2015; Fan et al., 2016; Mavromatis et al., 2016, 2020), but is almost the same to both the seasonal variability and absolute values observed in the large catchment of the Yenisei River (-1.13‰ to -0.96‰, Hindshaw et al., 2019).

Clear seasonal variation in $\delta^{26}Mg_{rw}$ in the middle Yellow River was observed, with values remaining relatively high (-1.04 ± 0.03‰) until the storm event where $\delta^{26}Mg_{rw}$ decreased from -1.09‰ to -1.20‰. $\delta^{26}Mg_{rw}$ values then returned to the preceding values within three weeks and eventually reached

-0.98‰ one month after the storm event (Fig. 2). After the monsoon, the $\delta^{26}Mg_{rw}$ values slowly decreased from -1.10‰ to -1.17‰ about 3 months after the storm event. Then $\delta^{26}Mg_{rw}$ rebounded back to the initial values and remained at those values for the rest of the year (-1.04 ± 0.02‰). Fan et al. (2016) reported a $\delta^{26}Mg_{rw}$ of -1.03 ± 0.10‰ for water collected at the Longmen hydrological station in August 2012, consistent with our values obtained for samples LM13-36 to LM13-40 (from -0.98 ± 0.03‰ to -1.08 ± 0.04‰) also collected in August but 2013. This similarity supports a seasonal consistency between two years for $\delta^{26}Mg_{rw}$ in the middle Yellow River.

Variations in $\delta^{26}Mg_{rw}$ showed patterns similar to those of the $^{87/86}Sr$ and Mg/Ca ratios at the seasonal scale in the middle Yellow River. However, all parameters show distinct responses to the storm event and in mid-November (Figs. 2 and S3). Notably, there were obvious low Mg and Sr isotopic compositions in mid-November (three months after the storm event), presumably resulting from a lag in the subsurface water transport (defined as hydrological hysteresis (Fig. 2), see discussion below; Andermann et al., 2012; Wanner et al., 2014; Liu et al., 2015; Emberson et al., 2016).

The average $\delta^{26}Mg$ of the rainwater ($\delta^{26}Mg_{rain}$) samples was -1.09‰, and the sewage water showed a $\delta^{26}Mg$ of -0.84‰. The sequential extraction experiment of 5 loess samples provided $\delta^{26}Mg$ for the evaporite, carbonate, and silicate components of the loess ($\delta^{26}Mg_{evap}$, $\delta^{26}Mg_{carb}$, and $\delta^{26}Mg_{sil}$), determined to be -1.11 ± 0.44‰, -1.58 ± 0.95‰, and -0.21 ± 0.19‰, respectively. All these numbers fall within the range of reported $\delta^{26}Mg$ for evaporite, carbonate, and silicate rocks (e.g., Teng, 2017, Fig. S1). The inferred $\delta^{26}Mg_{sil}$ is similar to that of the UCC (-0.22‰, Li et al., 2010; Teng et al., 2010; Teng, 2017).

5 Discussion

5.1. Mg fluxes in the Yellow River

Rivers export terrestrial Mg to the oceans either as dissolved load (Mg_{rw}), or as solid (Mg_{SPM}). Equations below are employed to determine the proportion of these two major forms of riverine Mg (Gaillardet et al., 2014; Gou et al., 2019b):

$$Mg_{rw}\ (\%) = \frac{Mg_{rw}\, flux}{Mg_{rw}\, flux + Mg_{SPM}\, flux} \times 100 \qquad \text{Eq (2)}$$

$$Mg_{SPM}\ (\%) = 100\% - Mg_{rw} \qquad \text{Eq (3)}$$

where the Mg_{rw} flux and Mg_{SPM} flux are given in t/yr (Fig. 2). The Mg_{rw} flux is the product of $[Mg]_{rw}$ and the corresponding weekly average Q_w as gauged (generally, three times/day) in the sampling site. Similarly, the Mg_{SPM} flux is calculated by multiplying the [Mg] in SPM and the corresponding weekly average SPM flux. In the middle Yellow River in 2013, Mg was primarily transported by the dissolved load (65.4%; Fig. S4). In the monsoon seasons, a higher percentage of river Mg was transported as solid. It is noteworthy that during the ice melting and the storm event intervals, the fraction of Mg transported as solids increased dramatically (up to 98%, Fig. S4). ~45% of the total dissolved Mg was transported during the monsoon seasons, with the 4-days storm event accounting for 2% of the annual flux (Fig. S4). Note that these estimates do not account for potential variability of Mg concentration and SPM with depth, although the middle Yellow River water appears homogeneous with respect to Li and Ba concentrations and isotopes of SPM in depth (Gou et al., 2019b, 2020). Such homogeneity should be applicable to Mg because Mg is a major ion therefore less likely affected by distribution, so our estimated Mg_{SPM} flux is likely accurate. Both the dissolved Mg and Sr flux in the Yellow River were exponential related to the PER, suggesting that chemical weathering is tightly related to physical erosion (Fig. 3).

5.2 Sources of dissolved Mg

Dissolved Mg sources in river waters include atmospheric input, anthropogenic input, and rock dissolution (Tipper et al., 2006b, 2008, 2012a, b; Brenot et al., 2008; Pogge von Strandmann et al., 2008b, 2014; Wimpenny et al., 2011; Opfergelt et al., 2012; Lee et al., 2014; Fan et al., 2016; Zhang et al., 2019; Hindshaw et al., 2019; Mavromatis et al., 2020). Hereafter attempts were made to discern the contributors to Mg_{rw} in the middle Yellow River.

5.2.1 Limited atmospheric input

Evaluation of atmospheric Mg inputs ($[Mg]_{atmo}$) was based on the Mg/Cl ratio (0.44 ± 0.27 mol/mol) of three rainwater samples and the reported evapotranspiration correction factor (*F*) in the middle CLP area of 1.76 (*F* ranges from 1.61 to 1.90, Zhang et al., 2015). We estimated that the $[Mg]_{atmo}$ is equal to 83.9 ± 50.2 μmol/L, which is 4%-8% of the total dissolved Mg (Fig. S5). This is a rather high contribution compared with that reported for other continental settings such as the Alps (0.6%, Millot et al., 2003; Tipper et al., 2012a), but it is low by comparison with islands such as Puerto Rico (71%-93%, Chapela Lara et al., 2017). These observations demonstrate that the contribution of atmospheric input to riverine Mg to the river dissolved Mg load strongly depends on the locations.

The δ^{26}Mg of rainwater samples were relatively homogeneous, -1.09‰ ± 0.03 (Table 2), within the range of the values reported elsewhere (e.g., −0.70 ‰ to −1.59‰; Riechelmann et al., 2012b; Tipper et al., 2010, 2012a; Teng et al., 2010; Fries et al., 2019), and were statistically different from the composition of a pure seawater-derived aerosol expected to be around -0.83‰ (Foster et al., 2010; Teng, 2017). The lighter Mg isotopic composition of the atmospheric contribution in the middle Yellow River basin is rather similar to the δ^{26}Mg of continental evaporites (average -1.11‰, Table S2). The maximum atmospheric input (8%) to the dissolved load combined to a maximum Mg isotopic difference (0.11‰) between the $\delta^{26}Mg_{rw}$ and $\delta^{26}Mg_{rain}$ implies that the atmospheric correction of the $\delta^{26}Mg_{rw}$ would induce a change < 0.01‰. Therefore, no corrections were applied here.

5.2.2 Insignificant anthropogenic inputs

Anthropogenic activities within the upper and middle Yellow River basin are dominated by sparse agriculture (Chen et al., 2003) without considerable industry. As our dataset showed that NO_3^- concentration in the middle Yellow River is higher than in typical pristine river waters, we assumed that all NO_3^- originates from fertilizers there (Chen et al., 2003; Zhang et al., 2015; Fan et al., 2016; Gou et al., 2019b). Using a typical NO_3/Na ratio of 7 ± 3 for fertilizer inputs (Roy et al., 1999; Chetelat et al., 2008), together with the Mg/Na molar ratio (~0.01) of the sewage water samples (Table S2) for the composition of anthropogenic inputs, we estimated the Mg anthropogenic input in the middle Yellow River to be between 0.3% and 0.8% (Fig. S5). In addition, the Mg isotopic composition of the anthropogenic input (-0.84 ± 0.04‰, defined as $\delta^{26}Mg_{anth}$) was higher than those of all the river water samples. In this case, during the monsoon season when agriculture prevails, we would observe a quite high $\delta^{26}Mg_{rw}$ value if the anthropogenic input were significant, which was not observed. As a result, anthropogenic input is negligible in the middle Yellow

River, likely because (1) Mg is the eighth abundant element in crust; (2) Mg is rarely a primary component of fertilizers; and (3) agricultural activity is sparse within the upper and middle Yellow River drainage basin (e.g., Chen et al., 2006a; Zhang et al., 2015; Fan et al., 2016).

5.2.3. Negligible contribution from biomass decay

Mg is one of the most important rock-derived nutrients, such that its incorporation in the biomass is associated with enrichment in light Mg isotopes in residual waters (Black et al., 2008; Bolou-Bi et al., 2009; Pokharel et al. 2018). In the Yellow River basin, crops growth rates are high during the monsoon seasons due to temperate climate and intense rainfall (Chen et al., 2003). However, we first note that biomass is very sparse in the upper and middle Yellow River basin due to the (semi-)arid condition and low temperature (Chen et al., 2003; Zhang et al., 2015; Fan et al., 2016; Gou et al., 2019b). Second, biological uptake tends to prefer both the heavy and light Mg isotopes (e.g., Bolou-Bi et al., 2010; Opfergelt et al., 2014; Balland-Bolou-Bi et a., 2019). If biological uptake were a driver of the dissolved Mg budget in the Yellow River, we would expect a varying $\delta^{26}Mg_{rw}$ values during the monsoon season when biomass growth is at its maximum, and an opposite $\delta^{26}Mg_{rw}$ values to monsoon season in the autumn when organic matter decays across the catchment (Chen et al., 2003). As none are observed, biological uptake is inferred to have a negligible effect on $\delta^{26}Mg_{rw}$ in the Yellow River basins. Thus, seasonal nutrient cycling is not important enough to affect the Mg cycle in the middle Yellow River basin.

Negligible biomass cycling to Mg in the middle Yellow River basin (Zhang et al., 2015; Fan et al., 2016) is consistent with observations elsewhere (Tipper et al., 2008, 2012b; Wimpenny et al., 2011; Lee et al., 2014; Dessert et al., 2015), although this contradicts results from the montane forest ecosystem of the Southern Sierra Critical Zone Observatory where over 50% Mg is taken up during plant growth (Uhlig et al., 2017). One possible reason for such difference could be related to the timing and kinetic of Mg turnover in plants.

5.2.4. Carbonate and silicate dissolution dominate the Mg budget in the Yellow River

As a major element in both carbonates and silicate minerals, river dissolved Mg is thought to be mainly derived from carbonate and silicate dissolution (Tipper et al., 2006c, 2012a, b; Pogge von Strandmann et al., 2008b, 2014; Brenot et al., 2008; Wimpenny et al., 2011; Lee et al., 2014; Dessert et al., 2015; Fan et al., 2016; Zhang et al., 2019; Fries et al., 2019; Zhao et al., 2019; Mavromatis et al., 2020). However, as the loess in the Yellow River basin contains ~5-10% evaporites (Zhang et al., 2020; Liu and Ding, 1998; Yokoo et al., 2004; Zhang et al., 1995, 1990), the contribution of evaporite dissolution to dissolved Mg in the middle Yellow River water chemistry must be quantified (Fan et al., 2016).

Since evaporites are more soluble than carbonates and silicates (e.g., Meybeck, 1987) and thus could contribute significant to dissolved Mg in the middle Yellow River (Zhang et al., 1990). Considering that the calculated dissolved Ca derived from evaporites in the middle Yellow River is 717 ± 180 μmol/L (Zhang et al., 2015) and using a typical molar Mg/Ca ratio of 0.099 ± 0.034 for evaporite minerals (Table S3, Yokoo et al., 2004; Zhang et al., 2020) contained of loess in the CLP, Mg derived from evaporites accounts for ~7% (ranging from 4.2% to 9.7%) of the dissolved Mg in the Yellow River water. In addition, Mg retrieved in the evaporite fraction of our sequential extraction experiments has a similar δ^{26}Mg value ($\delta^{26}Mg_{evap}$ = -1.11 ± 0.44‰) to that of the river water ($\delta^{26}Mg_{rw}$ from -0.98% to -1.20%), making it highly unlikely that evaporite dissolution has a discernible effect on the seasonal $\delta^{26}Mg_{rw}$ values in the middle Yellow River (Fig. S6).

Altogether, neither rain, anthropogenic, biological cycling, nor evaporites can contribute more than 20% of the dissolved Mg in the middle Yellow River, such that the remaining Mg derives from carbonate and silicate dissolution. This is consistent with that the lithology of the CLP which is made up of carbonated loess, with carbonates typically accounting for 8-20% of the loess (Kukla, 1987; Liu and Ding, 1998). Therefore, carbonate dissolution has a significant impact on the water chemistry in the Yellow River (Zhang et al., 2015). Initial attempts were made to quantify the contribution of carbonate *vs.* silicate dissolution to total dissolved Mg in the middle Yellow River by using a typical $(Mg/Na)_{sil}$ ratio of 0.54 (0.52–0.57, Gaillardet et al., 1999; Wu et al., 2005; Zhang et al., 2015). Results showed that the fraction of carbonate-sourced Mg (~$43^{+35}_{-32}\%$) is roughly equal to that of silicate-sourced Mg (~$43^{+30}_{-33}\%$, Fig. S5). However, this approach is unable to disclose the role of prior calcite precipitation (PCP), recognized to be a significant process impacting riverine chemistry in the CLP of the Yellow River (Li and Li, 2013). Furthermore, dissolved Mg once into river starts fractionation undiscernibly regardless its origin sources. We thus use Mg/Sr ratios later in the discussion, and return to this topic in section 5.3.1 (Figs. 4 and 5).

The Sr isotope ratios can serve as a conservative tracer of solute sources, as Sr isotope mass-dependent fractionation is normalized during data reduction. We thus employed the $^{87}Sr/^{86}Sr$ and Mg/Sr molar ratios of the loess from Yokoo et al. (2004), Yang et al. (1997, 2000) and Wu et al. (2005) as the lithological end members (evaporite, carbonate, and silicate). During the monsoon seasons, the correlation between $^{87}Sr/^{86}Sr$ and Mg/Sr showed that a mix of "carbonate of the upper reaches" and "Mg rich silicate of loess" with carbonate from loess acts as the first-order control on the Yellow River hydrochemistry (Fig. 4). This observation is in stark contrast with the lack of relationships between $^{87}Sr/^{86}Sr$ and Mg/Sr ratios during the dry seasons, indicating that source effects alone cannot completely explain the Mg budget during the dry seasons. It is because internally normalized Sr isotope ratios would not reveal Sr removal, while the removal of Mg by both 1) PCP (Li and Li, 2013; Yang et al., 2015) and 2) clay formation likely as a subordinate control on the Mg/Sr and Mg isotopes in the middle Yellow River (Fig. S7). We return to this feature later in the section 5.3.1.

More generally, taking the whole dataset into account, the significant ($p < 0.01$) covariation between $^{87}Sr/^{86}Sr$ and Mg/Sr (Fig. 4) supported: 1) a binary mixing between carbonate and silicate dissolution as the first order of control on $^{87}Sr/^{86}Sr$ ratios; 2) temporal variation in the fractional contributions of the two end members, and 3) the fact that the end members retrieved during our leaching experiments do not completely explain the mixing array (Fig. 4). In particular, one additional end member can be identified as the carbonate contribution from the upper Yellow River basin. There, carbonate dissolution accounts for 60% of the TDS (Li et al., 2018) at an $^{87}Sr/^{86}Sr$ ratio of ~0.71000 (Wu et al., 2005). As the upper Yellow River supplies ~1/3 of the TDS of the middle Yellow River (see section 4.1), the contribution of carbonate dissolution in the upper reaches cannot be neglected for the dissolved Mg budget of the middle reaches. In addition, we note that Mg-rich silicate minerals (*e.g.,* chlorite) may contribute to riverine Mg significant (Yokoo et al., 2004), meaning that some of the high Mg/Sr ratios observed in the riverine data (Figs. 2, 4 and S2) could be explained by the weathering of Mg-rich silicate minerals. With these two additional end members, the observed variation in ranges of $^{87}Sr/^{86}Sr$ and Mg/Sr ratios can be explained by mixing between silicates and carbonates both from upper and middle reaches of the Yellow River (Fig. 4). Altogether, Sr isotopes disclose a broad shifting proportion of weathering product between silicate and carbonate seasonally, while Mg isotopes seem revealing more details involved in weathering processes.

5.3 The role of PCP and clay formation on Mg isotopes

The seasonal $\delta^{26}Mg$ variation in the Yellow River depends on both 1) the relative contribution of silicate and carbonate rocks to the dissolved Mg budget, and 2) the processes affecting Mg once solubilized from minerals. First, to test for the role of lithological mixing on Mg isotopes, we derived the corresponding $\delta^{26}Mg$ constrained by our leaching experiments and summarized in Table S3 (Fan et al., 2016; Teng, 2017, Fig. S1). Mixing relationships between end member compositions ($\delta^{26}Mg$ versus Sr/Mg) further confirm that the dissolution of carbonate and silicate rocks are the primary control on dissolved Mg and Sr in the middle Yellow River, with approximately the same contribution for carbonate and silicate (*i.e.* ~40-50% each, Figs. 4 and 7), similar to estimates derived from elemental ratios alone (Fig. S5). Therefore, a combined dissolution of Mg from carbonate and silicate followed first by PCP (carbonate precipitation), and then by clay formation can fully explain the observation.

5.3.1 Quantifying the PCP fractionation on dissolved Mg isotopes

In rivers, the preferential removal of Ca relative to Sr and Mg during PCP generates a co-variation of the dissolved Sr/Ca and Mg/Ca ratios (Li and Li, 2013; Wassenburg et al., 2020; Yang et al., 2015, Fig. 5). Variations in river dissolved Mg/Ca and Sr/Ca ratios in response to the precipitation of secondary carbonate can be described by Rayleigh distillation following (Elderfield et al., 1996; Sinclair, 2011; Wassenburg et al., 2020):

$$[Sr/Ca]_{rw} = [Sr/Ca]_{initial} \times f^{\,DSr-1} \qquad \text{Eq (4)}$$

$$[Mg/Ca]_{rw} = [Mg/Ca]_{initial} \times f^{\,DMg-1} \qquad \text{Eq (5)}$$

where the $[Sr/Ca]_{initial}$ and $[Mg/Ca]_{initial}$ are the ratios of Sr and Mg to Ca in the "initial" waters after mineral dissolution and "before" secondary carbonate precipitation; D_{Sr} and D_{Mg} are the trace element distribution coefficient of Sr and Mg (e.g., Elderfield et al., 1996; Sinclair, 2011; Wassenburg et al., 2020), and f is the fraction of initial Ca remaining in river water after the precipitation of secondary carbonate. The Eqs. (4) and (5) can be simplified to:

$$[Sr/Ca]_{rw} = k \times [Mg/Ca]^{n}_{solution} \qquad \text{Eq (6)}$$

where n is equal to $(D_{Sr}-1)/(D_{Mg}-1)$.

The equation 6 can then be fitted to actual hydro-geochemical data to retrieve a best-fit value for n. Using our whole dataset of the middle Yellow River, the Sr/Ca and Mg/Ca ratios displayed a poor correlation ($r^2 = 0.47$), yielding a n value that is inconsistent with that expected for the PCP (Fig. 5). However, during the dry seasons (samples LM13-1 to 25 and LM13-56 to 60), the Sr/Ca and Mg/Ca ratios were well correlated ($r^2 = 0.93$, $p < 0.01$) and yield an n value of 1.064 ± 0.24 (Fig. 5), in line with the range of the theoretical ~0.85-1.45 associated with the PCP (Sinclair et al., 2012; Wassenburg et al., 2020).

Despite the fact that the PCP might have slightly modified the Mg content of river water, we can now determine the relative contribution of carbonate and silicate dissolution to the "initial" Mg dissolved budget from the combination of laws describing the evolution of water under the effect of PCP, and others describing the mixing of different sources. Using the above-determined coefficients for Mg, Ca, and Sr partitioning during the PCP in the middle Yellow River, the evolution of the composition of a water parcel under the effect of PCP can be described by:

$$\ln(1000{*}\mathrm{Sr/Ca})_{\mathrm{PCP}} = (1.064 \pm 0.24) \times \ln(\mathrm{Mg/Ca}) + (2.116 \pm 0.02) \qquad \text{Eq (7)}$$

whereas conservative mixing between carbonate and silicate dissolution can be written as below:

$$\ln(\mathrm{Sr/Ca})_{\mathrm{mixing}} = (f_{\mathrm{Sr}}(\mathrm{Sr_{carb}} - \mathrm{Sr_{sil}}) + \mathrm{Sr_{sil}})/(f_{\mathrm{Sr}}(\mathrm{Ca_{carb}} - \mathrm{Ca_{sil}}) + \mathrm{Ca_{sil}}) \qquad \text{Eq (8)}$$

$$\ln(\mathrm{Mg/Ca})_{\mathrm{mixing}} = (f_{\mathrm{Mg}}(\mathrm{Mg_{carb}} - \mathrm{Mg_{sil}}) + \mathrm{Mg_{sil}})/(f_{\mathrm{Mg}}(\mathrm{Ca_{carb}} - \mathrm{Ca_{sil}}) + \mathrm{Ca_{sil}}) \qquad \text{Eq (9)}$$

where f_{Sr} and f_{Mg} are the amounts of dissolved proportions of Sr and Mg relative to whole Ca from carbonates (Li and Li, 2013; Yang et al., 2015).

Equating the right-hand sides of Eqs. (7) and (8) and then employing Eq. (9) to our data returns an f_{Mg} of ~40 ± 11%, confirming that carbonate dissolution contributes ~40 ± 11% to Mg in the dry seasons as inferred from elemental constraints (Figs. 5 and S5). Note that variation in Mg/Sr of river waters is probably a result of mixing between calcite and dolomite dissolution (Fig. 5).

We then estimated the influence of the PCP on river dissolved Mg isotope signatures in the middle Yellow River. To do so, we used a Rayleigh distillation equation:

$$\delta^{26}Mg_{rw} = \delta^{26}Mg_{pre\text{-}PCP} + 1000 \times (g^{(\alpha-1)} - 1) \qquad \text{Eq (10)}$$

where $g = f \times f^{(DMg-1)}$, f is the amount of Ca remaining in the fluid after the PCP (Eqs. 4 and 5). Comparing dry season $(Mg/Ca)_{rw}$ to $(Mg/Ca)_{mixing}$, ~80% Ca has been lost through the PCP (Fig. 5), corresponding to a Mg loss of 5.6%.

The Mg isotope fractionation factors associated with the PCP (α_{PCP}) deduced from experiments were ranged from 0.9965 to 0.9985, depending on the carbonate precipitation rate (Galy et al. 2002; Mavromatis et al., 2013; Saenger et al., 2014). We here used this range to model PCP trends in the middle Yellow River based on Eq. 10.

The actual values of the partition coefficients D_{Mg} and D_{Sr} are related to a number of factors, such as carbonate precipitation rate, water Sr/Ca and Mg/Ca ratios, and temperature (Wassenburg et al., 2020). Considering the fact that in winter waters of the middle Yellow River are highly oversaturated waters, which mostly likely accelerates PCP, we used a D_{Mg} value of 0.07 (Wassenburg et al., 2020), corresponding to a D_{Sr} of 0.01 according to Eq. (7) (Sinclai, 2011; Sinclai et al., 2012; Li and Li 2013; Mavromatis et al., 2013; Yang et al., 2015; Wassenburg et al., 2020).

In the model, $\delta^{26}Mg_{pre\text{-}PCP}$ is the "initial" Mg isotope composition of waters, i.e. before the PCP occurs, and is derived from conservative mixing equations (Figs. 4, 5 and 7). Around 1/3 of the TDS of the middle Yellow River is derived from the upper Yellow River (60% from carbonates and 40% from silicates (Li et al., 2018), such that loess-derived Mg accounts for the remaining TDS of the middle Yellow River, with carbonate contributing 40% and silicate 60%. Considering that the $\delta^{26}Mg$ signature of silicates and carbonates from the upper reaches are to be -0.22‰ and -2.2‰, respectively (Fan et al., 2016), we obtained a $\delta^{26}Mg_{pre\text{-}PCP}$ value of -1.03‰ and a Sr/Mg of 7.44 in the dry seasons (Fig. 7). Similarly, given the elevated contribution of carbonate in the wet seasons, we estimated that the $\delta^{26}Mg_{pre\text{-}PCP}$ was -1.18‰ and Sr/Mg = 8.14 (Figs. 4 and 7). This is a first-order approximate quantification, leaving alone the uncertainties related with (1) the relative contributions of carbonate and silicate dissolution (Figs. 7 and S5) and (2) seasonal variability of the solute contribution from the upper Yellow River.

Using these constraints, we modelled that the removal of Mg during the PCP would approximately raise the $\delta^{26}Mg_{rw}$ of the water by ~0.17‰ to 0.39‰ depending on the D_{Mg} and fractionation factor values associated with the PCP (Fig. 7). Since most monsoon waters were supersaturated with respect to calcite, we thus also draw the PCP trend for the wet seasons (Fig. 7). The results showed that although the PCP fractionates Mg isotopes by ~0.17‰-0.39‰ compared to “initial” waters but lead to a positive trend in $\delta^{26}Mg_{rw}$ and Sr/Mg, PCP doesn’t dominate riverine Mg isotopes. Rather, we suggested that clay formation dominated $\delta^{26}Mg_{rw}$ in the middle Yellow River (Fig. 7).

5.3.2 Clay formation dominates dissolved Mg isotopes

After the PCP, Mg isotopes can be fractionated by clay formation, with a fractionation factor experimentally obtained as 1.00050-1.00075 (α_{clay}, Wimpenny et al., 2010, Fig. 7). Though the fractionation factors employed here are opposite to that Hindshaw et al. (2020), who argued that due to the Mg-O band length, clay may favor light Mg, however, averages of the reported $\delta^{26}Mg$ of soil (-0.20 ± 0.30‰), sediment (-0.09 ± 0.29‰), and SPM (0.32 ± 0.10‰)

globally are all isotopically heavier than the UCC (Fig. S1, Li et al., 2010; Teng, 2017), indicating that formation of clays may generally favor heavy Mg globally (Fig. S1). Therefore, we employed here the fractionation factors (α_{clay}, 1.00050-1.00075).

Using Eq. 10 with this range of the α_{clay} values, dissolution of silicate minerals alone followed by clay formation is an unlikely scenario to explain the observation on Mg isotopes in the middle Yellow River, as it would result a far higher $\delta^{26}Mg_{rw}$ than the observed data, regardless of the α_{clay} values prevailing during clay formation (Fig. 7). Alternatively, during the dry seasons, combined contribution of Mg from carbonate (~40%) and silicate (~60%) followed first by the PCP, and then by clay formation can fully explain the field observations. For example, using a 60%-40% silicate-carbonate mixture of Mg for the "initial" (before the PCP) composition of dry season waters, the inferred fractionation factor for PCP is of 0.9985. Such a value is consistent with the current knowledge on Mg isotope fractionation during PCP, as α_{PCP} is known to be tightly related to precipitation rate. Indeed, when waters are highly overstaturated, as is the case in the middle Yellow River during the dry season (Zhang et al., 2015), a higher precipitation rate is expected (Galy et al. 2002; Mavromatis et al., 2013; Saenger et al., 2014). After PCP, $\delta^{26}Mg_{rw}$ could be additionally elevated to -1.03‰ to -0.86‰, due to clay formation modifying the $\delta^{26}Mg_{rw}$ and Mg/Sr ratios by removal of heavy Mg. Any value of α_{clay} between 1.0005 and 1.00075 can explain the observed $\delta^{26}Mg_{rw}$ in the dry seasons (Fig. 7).

In the monsoon seasons, the slightly shift in mixing proportions (50% carbonate and 50% silicate) result in a lower "initial" $\delta^{26}Mg_{rw}$ (Fig. 7); however, most of the samples in the monsoon season are still supersaturated with respect to calcite (only samples from the storm event and from mid-November are unsaturated), implying that PCP is most likely operating during the monsoon season. The $\delta^{26}Mg_{rw}$ values modified by PCP in the monsoon season *via* carbonate precipitation can then be fractionated by clay formation (Fig. 7). In particular, the $\delta^{26}Mg_{rw}$ during the storm event and in mid-November show the lowest values of 2013, which is consistent with undersaturation with respect to calcite during those periods and associated absence of PCP that could elevate $\delta^{26}Mg_{rw}$ (Figs. 7 and S7).

5.4 The role of subsurface water transport in generating time lags in river hydrochemistry

Over the year of 2013, there were lower values of both $\delta^{26}Mg$ and $^{87}Sr/^{86}Sr$ in the middle Yellow River during the storm event. Following the model above, these low isotopic values would be mainly the result of enhanced Mg-bearing carbonate dissolution (Figs. 6 and 7), likely caused by the supply of highly undersaturated rainwater to the loess surface and subsurface (Meybeck, 1987; Buhl et al., 2007). One of the most interesting observations is that during the low runoff period of mid-November, low Mg and Sr isotope values were also observed (Figs. 2 and 6). It is hard to attribute to the shift in weathering sources or fractionation. Being considered that much of the surface runoff from the storm event could be temporarily sequestered in the porous loess that makes up the subsurface of the central part of the Yellow River basin. Here, we suggested that when river discharge decreases in the dry season, such water pool stored in the loess would be delivered to the river channel and maintain discharge, bearing the Sr and Mg isotope signatures of the storm event. Based upon our data, such scenario would require a lag time of about 3 months (i.e., hysteresis, Fig. 2). In fact, significant water storage has also been inferred in groundwater in mountainous areas such as the Andes (Liu et al., 2015; Wanner et al., 2014) or in the Himalayas (Andermann et al., 2012; Emberson et al., 2016), with a ~3 months residence time broadly (Fig. 7, Wimpenny et al., 2011), thus in agreement with our observations.

5.5 Implications

Over the year of 2013, the flux-weighted mean riverine δ^{26}Mg value of the middle Yellow River is -1.05‰, which is identical within uncertainty (± 0.05‰) to the global river average (-1.09‰, Tipper et al., 2006c), indicating that the CLP region is a representative setting to study Mg isotope response to climatic shifts on the continental scale. Despite the strong climatic seasonality affecting the CLP, riverine Mg isotopes appeared to be strongly buffered, exhibiting only ~0.2‰ variability throughout the year. The only significant shift in dissolved Mg isotope composition in the middle Yellow River in 2013 occurred during an extreme storm event and its subsequent hysteresis. Given that in the Yellow River dissolved Mg isotopes are sensitive at the seasonal scale to enhanced carbonate dissolution in the CLP during particular hydrological periods, the Mg isotope composition of loess-paleosol archives could be related to cumulative monsoonal precipitation through loss of carbonate (i.e., monsoonal precipitation intensity), dynamically supporting the idea that Mg isotopes of loess-paleosols can document monsoonal precipitation intensity on the CLP (Ma et al., 2019).

We highlight that even there are strong variability in temperature or rainfall, only an ~0.2‰ change in river dissolved δ^{26}Mg occurs, which is hardly to cause a resolvable change in the ocean Mg isotope budget (Fries et al., 2019). Meanwhile, although the dissolution of different lithologies provides very different Mg isotope signals (~2.5‰), their mixing remains relatively constant throughout the year at the scale of large rivers (Mavromatis et al., 2020). Hence, changes in climate cause little enhancement of selective leaching of different rock types, and hence Sr and Mg isotopes, on the continental scale. Therefore, large rivers appear highly buffered, suggesting that their δ^{26}Mg could remain relatively stable over long time periods. Only extreme changes would be required to alter their Mg isotope ratios, which is an important constraint for modeling the long-term evolution of the ocean Mg isotope composition in the frame of paleo-environmental studies relying on δ^{26}Mg in marine sedimentary archives (Pogge von Strandmann et al., 2014; Higgins and Schrag, 2015; He et al., 2020), for example, snowball earth, OAE etc.

6 Conclusions

In order to elucidate the controls on Mg isotope fractionation in large river catchments, we investigated how riverine δ^{26}Mg is affected by chemical weathering and extreme hydrological events, using water samples collected weekly from the middle reaches of the Yellow River in 2013. The following conclusion was drawn.

1) Mg in the middle Yellow River was dominantly transported in the dissolved form (65%); ~45% of dissolved Mg was transported during the monsoon season, and 2% during a single storm event (4 days).

2) To the first order, conservative mixing of Mg derived from the dissolution of carbonate and silicate rocks controlled the riverine Mg isotope composition. During the dry season, the relative contributions of carbonate and

silicate dissolution were 40 ± 11% and 60 ± 11% to total riverine Mg, respectively; in the monsoon season, their proportions shifted to 50 ± 10% and 50 ± 10%.

3) Prior calcite precipitation (PCP) led to ~80% Ca loss and ~6% Mg loss from the dissolved load, resulting in a 0.17‰-0.39% fractionation of Mg isotopically. After the PCP, clay formation further led the residual solution towards lower values of both δ^{26}Mg and Sr/Mg ratios.

4) The seasonal variation in riverine dissolved Mg isotope composition (~0.2‰) was mainly due to a single storm event that provided unsaturated waters to the surface, which in turn enhanced carbonate dissolution. Temporary storage of water in the porous loess underlying led to a ~3 months delayed response of both Mg and Sr isotopes to such extreme events.

Acknowledgements: This work was financially supported by NSFC (41991322), the 2nd Tibetan Plateau Scientific Expedition and Research (2019QZKK0707), and ERC Consolidator grant 682760 to PPvS. Christian France-Lanord and Guillaume Paris at Centre de Recherches Pétrographiques et Géochimiques, Eric H. Oelkers, David J. Wilson, and Melissa J. Murphy at University College London (UCL), Kang-Jun Huang at Northwest University, and Xiaowei Jiang at China University of Geosciences are thanked for their insightful comments that benefited this manuscript. We are grateful to Chun-Yao Liu at UCL, Ying-Zeng Gong, Fengtai Tong, Huimin Yu, and Fang Huang at University of Science and Technology of China for their kind help and suggestions to the laboratory work and insightful discussion during manuscript preparation.

References

An, Y.J., Wu, F., Xiang, Y.X., Nan, X.Y., Yu, X., Yang, J.H., Yu, H.M., Xie, L.W., Huang, F., 2014. High-precision Mg isotope analyses of low-Mg rocks by MC-ICP-MS. Chem. Geol. 390, 9-21.

Andermann, C., Longuevergne, L., Bonnet, S., Crave, A., Davy, P., Gloaguen, R., 2012. Impact of transient groundwater storage on the discharge of Himalayan rivers. Nat. Geosci. 5, 127-132.

Balland-Bolou-Bi, C., Bolou-Bi, E.B., Vigier, N., Mustin, C., Poszwa, A., 2019. Increased Mg release rates and related Mg isotopic signatures during bacteria-phlogopite interactions. Chem. Geol. 506, 17-28.

Berner, R.A., Lasaga, A.C., Garrels, R.M., 1983. The carbonate-silicate geochemical cycle and its effect on atmospheric carbon-dioxide over the past 100 million years. Am. J. Sci. 283, 641-683.

Bizzarro, M., Paton, C., Larsen, K., Schiller, M., Trinquier, A., Ulfbeck, D., 2011. High-precision Mg-isotope measurements of terrestrial and extraterrestrial material by HR-MC-ICPMS–implications for the relative and absolute Mg-isotope composition of the bulk silicate Earth. J. Anal. Atom. Spectrom. 26, 565-577.

Black, J.R., Epstein, E., Rains, W.D., Yin, Q.Z., Casey, W.H., 2008. Magnesium-isotope fractionation during plant growth. Environ. Sci. Technol. 42, 7831-7836.

Bolou-Bi, E.B., Poszwa, A., Leyval, C., Vigier, N., 2010. Experimental determination of magnesium isotope fractionation during higher plant growth. Geochim. Cosmochim. Acta 74, 2523-2537.

Bolou-Bi, E.B., Vigier, N., Brenot, A., Poszwa, A., 2009. Magnesium isotope compositions of natural reference materials. Geostand. Geoanal. Res. 33, 95-109.

Bouchez J., von Blanckenburg F., Schuessler J.A., 2013. Modeling novel stable isotope ratios in the weathering zone. Am. J. Sci. 313, 267-308.

Brenot, A., Cloquet, C., Vigier, N., Carignan, J., France-Lanord, C., 2008. Magnesium isotope systematics of the lithologically varied Moselle river basin, France. Geochim. Cosmochim. Acta 72, 5070-5089.

Buhl, D., Immenhauser, A., Smeulders, G., Kabiri, L., Richter, D.K., 2007. Time series delta ^{26}Mg analysis in speleothem calcite: Kinetic versus equilibrium fractionation, comparison with other proxies and implications for palaeoclimate research. Chem. Geol. 244, 715-729.

Chakrabarti, R., Jacobsen, S.B., 2010. The isotopic composition of magnesium in the inner solar system. Earth Planet. Sci. Lett. 293, 349-358.

Chapela Lara, M., Buss, H.L., Pogge von Strandmann, P.A.E., Schuessler, J.A., Moore, O.W., 2017. The influence of critical zone processes on the Mg isotope budget in a tropical, highly weathered andesitic catchment. Geochim. Cosmochim. Acta 202, 77-100.

Chen, J., He, D., Cui, S., 2003. The response of river water quality and quantity to the development of irrigated agriculture in the last 4 decades in the Yellow River basin, China. Water Resour. Res. 39, 3. doi:10.1029/2001WR001234.

Chen, J., Ke, D., Zhao, X., Fukushima, Y., Taniguchi, M., 2006a. Characteristics of sediment and nutrient flows in the lower reach of the Yellow River. Iahs-Aish P. 308, 612-616.

Chen, J., Wang, F., Meybeck, M., He, D., Xia, X., Zhang, L., 2005. Spatial and temporal analysis of water chemistry records (1958-2000) in the Huanghe (Yellow River) basin. Glob. Biogeochem. Cy. 19, GB3016, doi:10.1029/2004GB002325.

Chen, J.S., Yu, T., Ongley, E., 2006b. Influence of high levels of total suspended solids on measurement of cod and bod in the Yellow River, China. Environ. Monit. Assess. 116, 321-334.

Chetelat, B., Liu, C.Q., Zhao, Z.Q., Wang, Q.L., Li, S.L., Li, J., Wang, B.L., 2008. Geochemistry of the dissolved load of the Changjiang Basin rivers: Anthropogenic impacts and chemical weathering. Geochim. Cosmochim. Acta 72, 4254-4277.

Choi, M.S., Ryu, J.S., Lee, S.W., Shin, H.S., Lee, K.S., 2012. A revisited method for Mg purification and isotope analysis using cool-plasma MC-ICP-MS. J. Anal. Atom. Spectrom. 27, 1955-1959.

Coath, C.D., Elliott, T., Hin, R.C., 2017. Double-spike inversion for three-isotope systems. Chem. Geol. 451, 78-89.

Dessert, C., Lajeunesse, E., Lloret, E., Clergue, C., Crispi, O., Gorge, C., Quidelleur, X., 2015. Controls on chemical weathering on a mountainous volcanic tropical island: Guadeloupe (French West Indies). Geochim. Cosmochim. Acta 171, 216-237.

Elderfield, H., 1996. A biomineralization model for the incorporation of trace elements into foraminiferal calcium carbonate. Earth Planet. Sci. Lett. 142, 409-423.

Emberson, R., Hovius, N., Galy, A., Marc, O., 2016. Chemical weathering in active mountain belts controlled by stochastic bedrock landsliding. Nat. Geosci. 9, 42-45.

Fan, B., Zhao, Z.-Q., Tao, F., Li, X., Tao, Z., Gao, S., He, M., 2016. The geochemical behavior of Mg isotopes in the Huanghe basin, China. Chem. Geol. 426, 19-27.

Foster, G.L., Pogge von Strandmann P.A.E., Rae J.W.B., 2010. Boron and magnesium isotopic composition of seawater. Geochem. Geophys. Geosys. 11. doi: 10.1029/2010gc003201

Gaillardet, J., Dupre, B., Louvat, P., Allegre, C.J., 1999. Global silicate weathering and CO_2 consumption rates deduced from the chemistry of large rivers. Chem. Geol. 159, 3-30.

Gaillardet, J., Viers, J., Dupre, B., 2014. Trace elements in river waters. In: Holland H.D. and Turekian K.K. eds.Treatise on Geochemistry, second ed. Elsevier, Oxford, pp. 195–235.

Galy, A., Bar-Matthews, M., Halicz, L., O'Nions, R.K., 2002. Mg isotopic composition of carbonate: insight from speleothem formation. Earth Planet. Sci. Lett. 201, 105-115.

Galy, A., Belshaw, N.S., Halicz, L., O'Nions, R.K., 2001. High-precision measurement of magnesium isotopes by multiple-collector inductively coupled plasma mass spectrometry. Int. J. Mass Spectrom. 208, 89-98.

Galy, A., France-Lanord, C., 1999. Weathering processes in the Ganges-Brahmaputra basin and the riverine alkalinity budget. Chem. Geol. 159, 31-60.

Galy, A., Yoffe, O., Janney, P.E., Williams, R.W., Cloquet, C., Alard, O., Halicz, L., Wadhwa, M., Hutcheon, I.D., Ramon, E., Carignan, J., 2003. Magnesium isotope heterogeneity of the isotopic standard SRM980 and new reference materials for magnesium-isotope-ratio measurements. J. Anal. Atom. Spectrom. 18, 1352.

Georg, R.B., Reynolds, B.C., West, A.J., Burton, K.W., Halliday, A.N., 2007. Silicon isotope variations accompanying basalt weathering in Iceland. Earth Planet. Sci. Lett. 261, 476-490.

Gou, L.-F., Jin, Z., Galy, A., Sun, H., Deng, L., Xu, Y., 2019a. Effects of cone combinations on accurate and precise Mg-isotopic determination using multi-collector inductively coupled plasma mass spectrometry. Rapid Commun. Mass Spectr. 33, 351-360.

Gou, L.-F., Jin, Z., Galy, A., Gong, Y.-Z., Nan, X.-Y., Jin, C., Wang, X.-D., Bouchez, J., Cai, H.-M., Chen, J.-B., Yu, H.-M., Huang, F., 2020. Seasonal riverine barium isotopic variation in the middle Yellow River: Sources and fractionation. Earth Planet. Sci. Lett. 531, 115990.

Gou, L.-F., Jin, Z., Pogge von Strandmann, P.A.E., Li, G., Qu, Y.-X., Xiao, J., Deng, L., Galy, A., 2019b. Li isotopes in the middle Yellow River: Seasonal variability, sources and fractionation. Geochim. Cosmochim. Acta 248, 88-108.

He, R., Ning, M., Huang, K., Ma, H., Shen, B., 2020. Mg isotopic systematics during early diagenetic aragonite-calcite transition: Insights from the Key Largo Limestone. Chem. Geol. 558, 119876.

Higgins, J.A., Schrag, D.P., 2015. The Mg isotopic composition of Cenozoic seawater-evidence for a link between Mg-clays, seawater Mg/Ca, and climate. Earth Planet. Sci. Lett. 416, 73-81.

Hin, R.C., Coath, C.D., Carter, P.J., Nimmo, F., Lai, Y.J., Pogge von Strandmann, P.A.E., Willbold, M., Leinhardt, Z.M., Walter, M.J., Elliott, T., 2017. Magnesium isotope evidence that accretional vapour loss shapes planetary compositions. Nature 549, 511-515.

Hindshaw, R.S., Tosca, R., Tosca, N.J. and Tipper, E.T., 2020. Experimental constraints on Mg isotope fractionation during clay formation: Implications for the global biogeochemical cycle of Mg. Earth Planet. Sci. Lett. 531, 115980.

Hindshaw, R.S., Teisserenc, R., Le Dantec, T. and Tananaev, N., 2019. Seasonal change of geochemical sources and processes in the Yenisei River: A Sr, Mg and Li isotope study. Geochim. Cosmochim. Acta 255, 222-236

Huang, F., Glessner, J., Ianno, A., Lundstrom, C., Zhang, Z.F., 2009. Magnesium isotopic composition of igneous rock standards measured by MC-ICP-MS. Chem. Geol. 268, 15-23.

Huang, K.-J., Teng, F.-Z., Wei, G.-J., Ma, J.-L., Bao, Z.-Y., 2012. Adsorption- and desorption-controlled magnesium isotope fractionation during extreme weathering of basalt in Hainan Island, China. Earth Planet. Sci. Lett. 359, 73-83.

Immenhauser, A., Buhl, D., Richter, D., Niedermayr, A., Riechelmann, D., Dietzel, M., Schulte, U., 2010. Magnesium-isotope fractionation during low-Mg calcite precipitation in a limestone cave - Field study and experiments. Geochim. Cosmochim. Acta 74, 4346-4364.

Jacobson, A.D., Zhang, Z., Lundstrom, C., Huang, F., 2010. Behavior of Mg isotopes during dedolomitization in the Madison aquifer, south Dakota. Earth Planet. Sci. Lett. 297, 446-452.

Jin, Z., You, C.-F., Yu, J., Wu, L., Zhang, F., Liu, H.-C., 2011. Seasonal contributions of catchment weathering and eolian dust to river water chemistry, northeastern Tibetan Plateau: Chemical and Sr isotopic constraints. J. Geophys. Res. 116, F04006, doi:10.1029/2011JF002002.

Kasemann, S.A., Pogge von Strandmann, P.A.E., Prave, A.R., Fallick, A.E., Elliott, T. Hoffmann, K.-H., 2014. Continental weathering following a Cryogenian glaciation: Evidence from calcium and magnesium isotopes. Earth Planet. Sci. Lett. 396, 66-77.

Kukla, G., 1987. Loess stratigraphy in central China. Quat. Sci. Rev. 6, 191-219.

Larsen, K.K., Trinquier, A., Paton, C., Schiller, M., Wielandt, D., Ivanova, M.A., Connelly, J.N., Nordlund, A., Krot, A.N., Bizzarro, M., 2011. Evidence for magnesium isotope heterogeneity in the solar protoplanetary disk. Astrophys. J. Lett. 735, 2. doi:Artn L3710.1088/2041-8205/735/2/L37.

Lee, S.-W., Ryu, J.-S., Lee, K.-S., 2014. Magnesium isotope geochemistry in the Han River, south Korea. Chem. Geol. 364, 9-19.

Li, L., Zhang, F., Jin, Z., Xiao, J., Gou, L.-F. and Xu, Y., 2020. Riverine Mg isotopes response to glacial weathering within the Muztag catchment of the eastern Pamir Plateau. Appl. Geochem. 118, 104626.

Li, W., Chakraborty, S., Beard, B.L., Romanek, C.S., Johnson, C.M., 2012. Magnesium isotope fractionation during precipitation of inorganic calcite under laboratory conditions. Earth Planet. Sci. Lett. 333, 304-316.

Li, W.Y., Teng, F.Z., Ke, S., Rudnick, R.L., Gao, S., Wu, F.Y., Chappell, B.W., 2010. Heterogeneous magnesium isotopic composition of the upper continental crust. Geochim. Cosmochim. Acta 74, 6867-6884.

Li, Y.H., Teraoka, H., Yang, T.S., Chen, J.S., 1984. The elemental composition of suspended particles from the Yellow and Yangtze Rivers. Geochim. Cosmochim. Acta 48, 1561-1564.

Liu, T.S., 1988. Loess in China. Beijing, 2nd edition, p. 224.

Liu, T.S., Ding, Z.L., 1998. Chinese loess and the paleomonsoon. Annu. Rev. Earth Planet. Sci. 26, 111-145.

Liu, X.-M., Wanner, C., Rudnick, R.L., McDonough, W.F., 2015. Processes controlling δ^{7}Li in rivers illuminated by study of streams and groundwaters draining basalts. Earth Planet. Sci. Lett. 409, 212-224.

Ma, L., Sun, Y., Jin, Z., Bao, Z., Zhang, P., Meng, Z., Yuan, H., Long, X., He, M., Huang, K.-J., 2019. Tracing changes in monsoonal precipitation using Mg isotopes in Chinese loess deposits. Geochim. Cosmochim. Acta 259, 1-16.

Mavromatis, V., Rinder, T., Prokushkin, A.S., Pokrovsky, O.S., Korets, M.A., Chmeleff, J., Oelkers, E.H., 2016. The effect of permafrost, vegetation, and lithology on Mg and Si isotope composition of the Yenisey River and its tributaries at the end of the spring flood. Geochim. Cosmochim. Acta 191, 32-46.

Meybeck, M., 1987. Global chemical-weathering of surficial rocks estimated from river dissolved loads. Am. J. Sci. 287, 401-428.

Opfergelt, S., Georg, R.B., Delvaux, B., Cabidoche, Y.M., Burton, K.W., Halliday, A.N., 2012. Mechanisms of magnesium isotope fractionation in volcanic soil weathering sequences, Guadeloupe. Earth Planet. Sci. Lett. 341, 176-185.

Pogge von Strandmann, P.A.E., 2008. Precise magnesium isotope measurements in core top planktic and benthic foraminifera. Geochem. Geophys. Geosys. 9. Q12015, doi:10.1029/2008GC002209.

Pogge von Strandmann, P.A.E., Burton, K.W., James, R.H., van Calsteren, P., Gislason, S.R., Sigfusson, B., 2008a. The influence of weathering processes on riverine magnesium isotopes in a basaltic terrain. Earth Planet. Sci. Lett. 276, 187-197.

Pogge von Strandmann, P.A.E., Burton, K.W., Opfergelt, S., Eiríksdóttir, E.S., Murphy, M.J., Einarsson, A., Gislason, S.R., 2020. Hydrothermal and cold spring water and primary productivity effects on magnesium isotopes: Lake Myvatn, Iceland. Front. Earth Sci. 8, 109. doi: 10.3389/feart.2020.00109.

Pogge von Strandmann, P.A.E., Frings, P.J., Murphy, M.J., 2017. Lithium isotope behaviour during weathering in the Ganges Alluvial Plain. Geochim. Cosmochim. Acta 198, 17-31.

Pogge von Strandmann, P.A.E., James, R.H., van Calsteren, P., Gislason, S.R., Burton, K.W., 2008b. Lithium, magnesium and uranium isotope behaviour in the estuarine environment of basaltic islands. Earth Planet. Sci. Lett. 274, 462-471.

Pogge von Strandmann, P.A.E., Olsson, J., Luu, T.-H., Gislason, S.R., Burton, K.W., 2019. Using Mg isotopes to estimate natural calcite compositions and precipitation rates during the 2010 Eyjafjallajökull eruption. Front. Earth Sci. 7, 6. doi: 10.3389/feart. 2019.00006.

Pogge von Strandmann, P.A.E., Opfergelt, S., Lai, Y.-J., Sigfusson, B., Gislason, S.R., Burton, K.W., 2012. Lithium, magnesium and silicon isotope behaviour accompanying weathering in a basaltic soil and pore water profile in Iceland. Earth Planet. Sci. Lett. 339, 11-23.

Pokharel, R., Gerrits, R., Schuessler, J.A., von Blanckenburg, F., 2019. Mechanisms of olivine dissolution by rock-inhabiting fungi explored using magnesium stable isotopes. Chem. Geol. 525, 18-27.

Ran, L.S., Lu, X.X., Sun, H.G., Han, J.T., Yu, R.H., 2015. Chemical denudation in the Yellow River and its geomorphological implications. Geomorphology 231, 83-93.

Riechelmann, S., Buhl, D., Schroeder-Ritzrau, A., Riechelmann, D.F.C., Richter, D.K., Vonhof, H.B., Wassenburg, J.A., Geske, A., Spoetl, C., Immenhauser, A., 2012a. The magnesium isotope record of cave carbonate archives. Clim. Past 8, 1849-1867.

Riechelmann, S., Buhl, D., Schroeder-Ritzrau, A., Spoetl, C., Riechelmann, D.F.C., Richter, D.K., Kluge, T., Marx, T., Immenhauser, A., 2012b. Hydrogeochemistry and fractionation pathways of Mg isotopes in a continental weathering system: Lessons from field experiments. Chem. Geol. 300, 109-122.

Roy, S., Gaillardet, J., Allegre, C.J., 1999. Geochemistry of dissolved and suspended loads of the Seine river, France: Anthropogenic impact, carbonate and silicate weathering. Geochim. Cosmochim. Acta 63, 1277-1292.

Ryu, J.-S., Vigier, N., Decarreau, A., Lee, S.-W., Lee, K.-S., Song, H., Petit, S., 2016. Experimental investigation of Mg isotope fractionation during mineral dissolution and clay formation. Chem. Geol. 445, 135-145.

Saenger, C., Wang, Z., 2014. Magnesium isotope fractionation in biogenic and abiogenic carbonates: implications for paleoenvironmental proxies. Quat. Sci. Rev. 90, 1-21.

Saito, Y., Yang, Z.S., Hori, K., 2001. The Huanghe (Yellow River) and Changjiang (Yangtze River) deltas: a review on their characteristics, evolution and sediment discharge during the Holocene. Geomorphology 41, 219-231.

Sinclair, D.J., 2011. Two mathematical models of Mg and Sr partitioning into solution during incongruent calcite dissolution. Chem. Geol. 283, 119-133.

Sinclair, D.J., Banner, J.L., Taylor, F.W., Partin, J., Jenson, J., Mylroie, J., Goddard, E., Quinn, T., Jocson, J. and Miklavič, B., 2012. Magnesium and strontium systematics in tropical speleothems from the Western Pacific. Chem. Geol. 294-295, 1-17.

Sikdar, J., Rai, V.K., 2017. Simultaneous chromatographic purification of Si and Mg for isotopic analyses using MC-ICPMS. J. Anal. Atom. Spectrom. 32, 822-833.

Tanimizu, M., 2008. Determination of Mg Isotopic composition of seawater with a rapid Mg purification technique. J. Nucl. Sci. Technol. 45, 51-54.

Teng, F.-Z., 2017. Magnesium isotope geochemistry. Rev. Mineral. Geochem. 82, 219-287.

Teng, F.-Z., Li, W.-Y., Rudnick, R.L., Gardner, L.R., 2010. Contrasting lithium and magnesium isotope fractionation during continental weathering. Earth Planet. Sci. Lett. 300, 63-71.

Teng, F.Z., Yin, Q.Z., Ullmann, C.V., Chakrabarti, R., Pogge von Strandmann, P.A.E, Yang, W., Li, W.Y., Ke, S., Sedaghatpour, F., Wimpenny, J., Meixner, A., Romer, R.L., Wiechert, U., Jacobsen, S.B., 2015. Interlaboratory comparison of magnesium isotopic compositions of 12 felsic to ultramafic igneous rock standards analyzed by MC-ICPMS. Geochem. Geophys. Geosys. 16, 3197-3209.

Tessier, A., Campbell, P.G.C., Bisson, M., 1979. Sequential extraction procedure for the speciation of particulate trace-metals. Anal. Chem. 51, 844-851.

Tipper, E.T., Bickle, M.J., Galy, A., West, A.J., Pomiès, C., Chapman, H.J., 2006a. The short term climatic sensitivity of carbonate and silicate weathering fluxes: Insight from seasonal variations in river chemistry. Geochim. Cosmochim. Acta 70, 2737-2754.

Tipper, E.T., Calmels, D., Gaillardet, J., Louvat, P., Capmas, F., Dubacq, B., 2012a. Positive correlation between Li and Mg isotope ratios in the river waters of the Mackenzie Basin challenges the interpretation of apparent isotopic fractionation during weathering. Earth Planet. Sci. Lett. 333-334, 35-45.

Tipper, E.T., Gaillardet, J., Louvat, P., Capmas, F., White, A.F., 2010. Mg isotope constraints on soil pore-fluid chemistry: Evidence from Santa Cruz, California. Geochim. Cosmochim. Acta 74, 3883-3896.

Tipper, E.T., Galy, A., Bickle, M.J., 2006b. Riverine evidence for a fractionated reservoir of Ca and Mg on the continents: Implications for the oceanic Ca cycle. Earth Planet. Sci. Lett. 247, 267-279.

Tipper, E.T., Galy, A., Bickle, M.J., 2008. Calcium and magnesium isotope systematics in rivers draining the Himalaya-Tibetan-Plateau region: Lithological or fractionation control? Geochim. Cosmochim. Acta 72, 1057-1075.

Tipper, E.T., Galy, A., Gaillardet, J., Bickle, M.J., Elderfield, H., Carder, E.A., 2006c. The magnesium isotope budget of the modem ocean: Constraints from riverine magnesium isotope ratios. Earth Planet. Sci. Lett. 250, 241-253.

Tipper, E.T., Lemarchand, E., Hindshaw, R.S., Reynolds, B.C., Bourdon, B., 2012b. Seasonal sensitivity of weathering processes: Hints from magnesium isotopes in a glacial stream. Chem. Geol. 312, 80-92.

Uhlig, D., Schuessler, J.A., Bouchez, J., Dixon, J.L., von Blanckenburg, F., 2017. Quantifying nutrient uptake as driver of rock weathering in forest ecosystems by magnesium stable isotopes. Biogeosciences 14, 3111-3128.

Walker, J.C.G., Hays, P.B., Kasting, J.F., 1981. A negative feedback mechanism for the long-term stabilization of Earth's surface temperature. J. Geophys. Res. 86, 9776-9782.

Wang, G.Q., Lin, Y.T., Liang, X.R., Liu, Y., Xie, L.W., Yang, Y.H., Tu, X.L., 2011. Separation of magnesium from meteorites and terrestrial silicate rocks for high-precision isotopic analysis using multiple collector-inductively coupled plasma-mass spectrometry. J. Anal. Atom. Spectrom. 26, 1878-1886.

Wang, H., Bi, N., Saito, Y., Wang, Y., Sun, X., Zhang, J., Yang, Z., 2010. Recent changes in sediment delivery by the Huanghe (Yellow River) to the sea: Causes and environmental implications in its estuary. J. Hydrol. 391, 302-313.

Wang, H., Yang, Z., Saito, Y., Liu, J.P., Sun, X., Wang, Y., 2007. Stepwise decreases of the Huanghe (Yellow River) sediment load (1950–2005): Impacts of climate change and human activities. Global Planet. Change 57, 331-354.

Wanner, C., Sonnenthal, E.L., Liu, X.-M., 2014. Seawater δ^7Li: A direct proxy for global CO_2 consumption by continental silicate weathering? Chem. Geol. 381, 154-167.

Wassenburg, J.A., Riechelmann, S., Schröder-Ritzrau, A., Riechelmann, D.F.C., Richter, D.K., Immenhauser, A., Terente, M., Constantin, S., Hachenberg, A., Hansen, M. and Scholz, D., 2020. Calcite Mg and Sr partition coefficients in cave environments: Implications for interpreting prior calcite precipitation in speleothems. Geochim. Cosmochim. Acta 269, 581-596.

West, A.J., Galy, A., Bickle, M., 2005. Tectonic and climatic controls on silicate weathering. Earth Planet. Sci. Lett. 235, 211-228.

Wimpenny, J., Burton, K.W., James, R.H., Gannoun, A., Mokadem, F., Gislason, S.R., 2011. The behaviour of magnesium and its isotopes during glacial weathering in an ancient shield terrain in West Greenland. Earth Planet. Sci. Lett. 304, 260-269.

Wimpenny, J., Gíslason, S.R., James, R.H., Gannoun, A., Pogge von Strandmann, P.A.E., Burton, K.W., 2010. The behaviour of Li and Mg isotopes during primary phase dissolution and secondary mineral formation in basalt. Geochim. Cosmochim. Acta 74, 5259-5279.

Wimpenny, J., Yin, Q.-Z., Tollstrup, D., Xie, L.-W., Sun, J., 2014. Using Mg isotope ratios to trace Cenozoic weathering changes: A case study from the Chinese Loess Plateau. Chem. Geol. 376, 31-43.

Xu, Y., Jin, Z., Gou, L.-F., Galy, A., Jin, C., Chen, C., Li, C. Deng, L. 2021. Carbonate weathering dominates magnesium isotopes in large rivers: Clues from the Yangtze River. Chem. Geol. 120677.

Yang, J., Chen, J., An, Z., Shields, G., Tao, X., Zhu, H., Ji, J., Chen, Y., 2000. Variations in $^{87}Sr/^{86}Sr$ ratios of calcites in Chinese loess: A proxy for chemical weathering associated with the East Asian summer monsoon. Palaeogeogr. Palaeoclimat. Palaeocl. 157, 151-159.

Yokoo, Y., Nakano, T., Nishikawa, M., Quan, H., 2004. Mineralogical variation of Sr–Nd isotopic and elemental compositions in loess and desert sand from the central Loess Plateau in China as a provenance tracer of wet and dry deposition in the northwestern Pacific. Chem. Geol. 204, 45-62.

Young, E.D., Galy, A., 2004. The isotope geochemistry and cosmochemistry of magnesium. Rev. Mineral. Geochem. 55, 197-230.

Young, E.D., Galy, A., Nagahara, H., 2002. Kinetic and equilibrium mass-dependent isotope fractionation laws in nature and their geochemical and cosmochemical significance. Geochim. Cosmochim. Acta 66, 1095-1104.

Yu, Y., Wang, H., Shi, X., Ran, X., Cui, T., Qiao, S., Liu, Y., 2013. New discharge regime of the Huanghe (Yellow River): Causes and implications. Cont. Shelf Res. 69, 62-72.

Zhang, D., Zhao, Z.-Q., Peng, Y., Fan, B., Zhang, L., Li, J., Chen, A., 2020. Sulfur cycling in the Yellow River and the sulfate flux to the ocean. Chem. Geol. 534, 119451.

Zhang, J., Huang, W.W., Letolle, R., Jusserand, C., 1995. Major-element chemistry of the Huanghe (Yellow-River), China - weathering processes and chemical fluxes. J. Hydrol. 168, 173-203.

Zhang, J., Huang, W.W., Shi, M.C., 1990. Huanghe (Yellow-River) and its estuary - sediment origin, transport and deposition. J. Hydrol. 120, 203-223.

Zhang, H., Jiang, X.-W., Wan, L., Ke, S., Liu, S.-A., Han, G., Guo, H., Dong, A., 2018. Fractionation of Mg isotopes by clay formation and calcite precipitation in groundwater with long residence times in a sandstone aquifer, Ordos Basin, China. Geochim. Cosmochim. Acta 237, 261-274.

Zhang, Q., Jin, Z., Zhang, F., Xiao, J., 2015. Seasonal variation in river water chemistry of the middle reaches of the Yellow River and its controlling factors. J. Geochem. Explor. 156, 101-113.

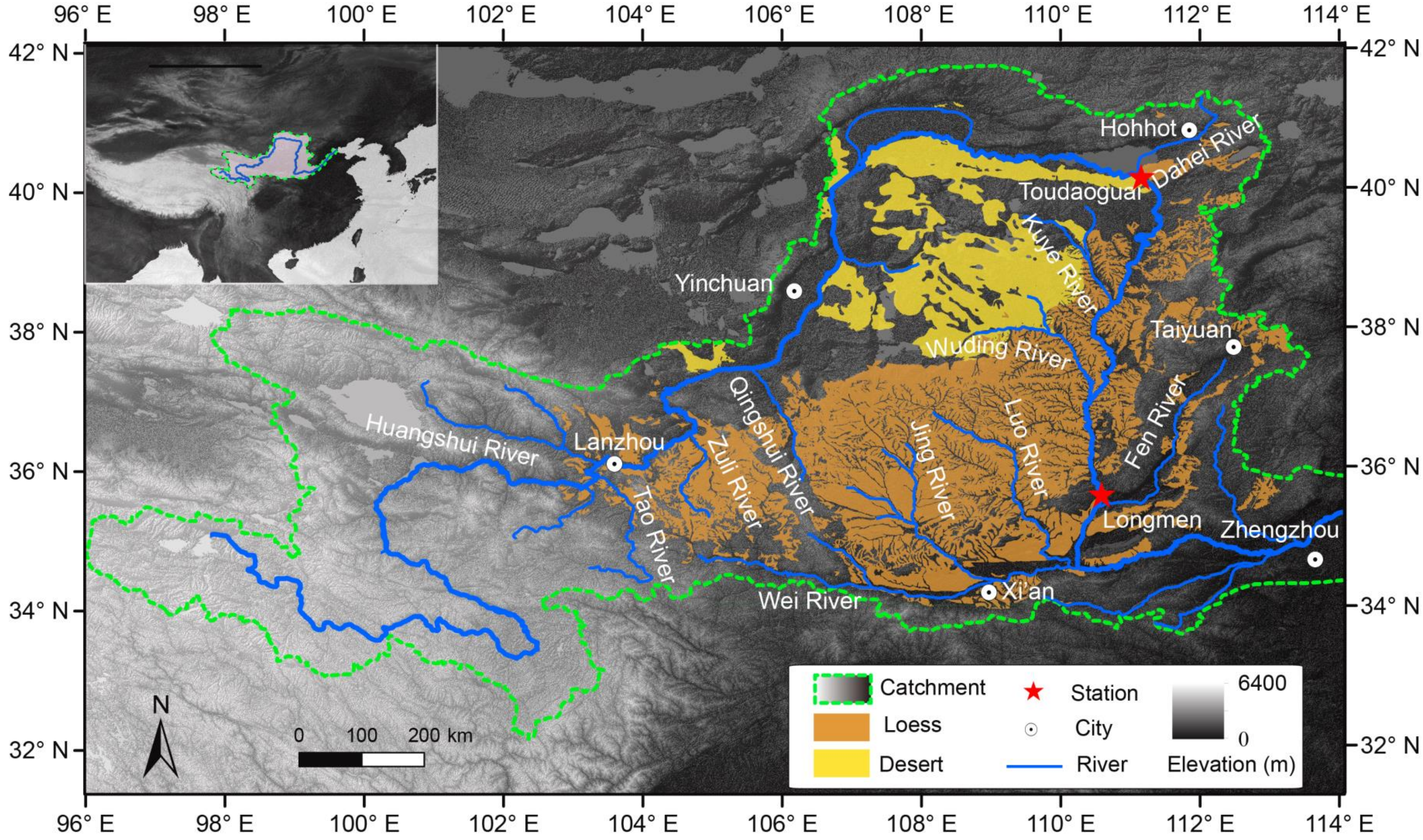
96° E
98° E
100° E
102° E
104° E
106° E
108° E
110° E
112° E
114° E
42° N
40° N
38° N
36° N
34° N
32° N
Hohhot
Dahei River
Toudaoguai
Kuye River
Yinchuan
Taiyuan
Wuding River
Qingshui River
Luo River
Fen River
Huangshui River
Lanzhou
Zuli River
Jing River
Tao River
Longmen
Zhengzhou
Xi'an
Wei River
N
0
100
200 km
Catchment
Station
6400
0
Elevation (m)
Loess
City
Desert
River

Figure 1 Map of the Yellow River drainage basin, with major tributaries and sampling locations (Toudaoguai and Longmen hydrological stations). Loess and desert dominate the lithology within the upper and middle reaches of the Yellow River basin. Inset map shows the whole Yellow River drainage basin.

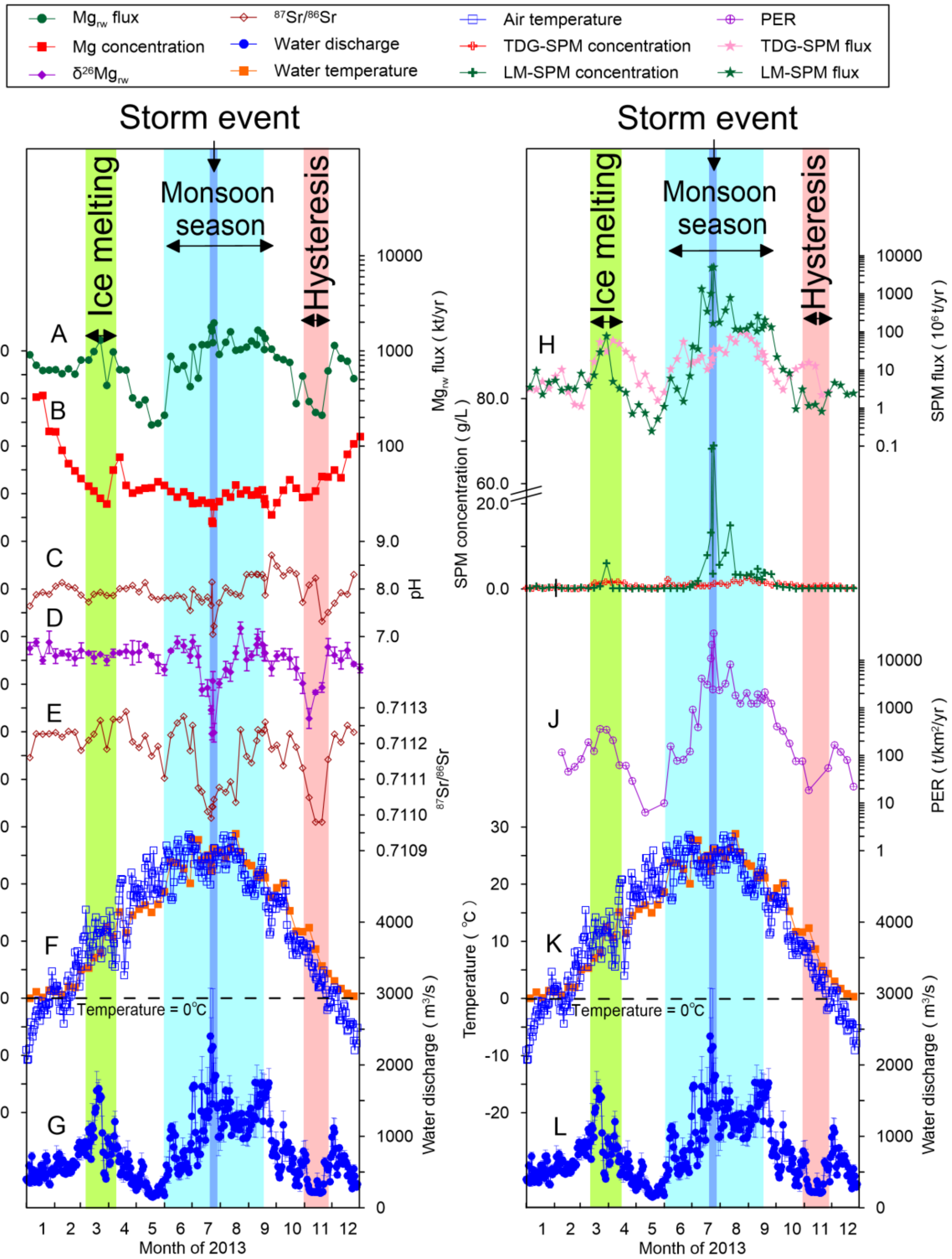

Figure 2 Date from 1st Jan. to 31th Dec., 2013, the number on x-Axis is at the middle of each month. (a) Mg^{2+} flux, (b) Mg^{2+} concentration, (c) pH, (d) δ^{26}Mg$_{rw}$ and (e) ^{87}Sr/^{86}Sr of river water collected weekly at the Longmen hydrological station over the whole year of 2013, along with (f, k) water and air temperatures, and (g, l) water discharge, (h) SPM flux, (i) concentration of SPM and (j) physical erosion rate (PER, from Zhang et al. (2015)) calculated

by weekly gauging, all showing obvious seasonal variations. Note that $\delta^{26}Mg_{rw}$ and $^{87}Sr/^{86}Sr$ exhibited similar patterns, with two spikes during the storm event and 3 months after its end (hydrological hysteresis). The intervals of ice melting (during 16th March and 13th April), monsoon season (From June to mid-September), a single storm event (22nd to 25th of July), and the period of hydrological hysteresis, shown as green, blue, dark blue, and red shaded areas, respectively.

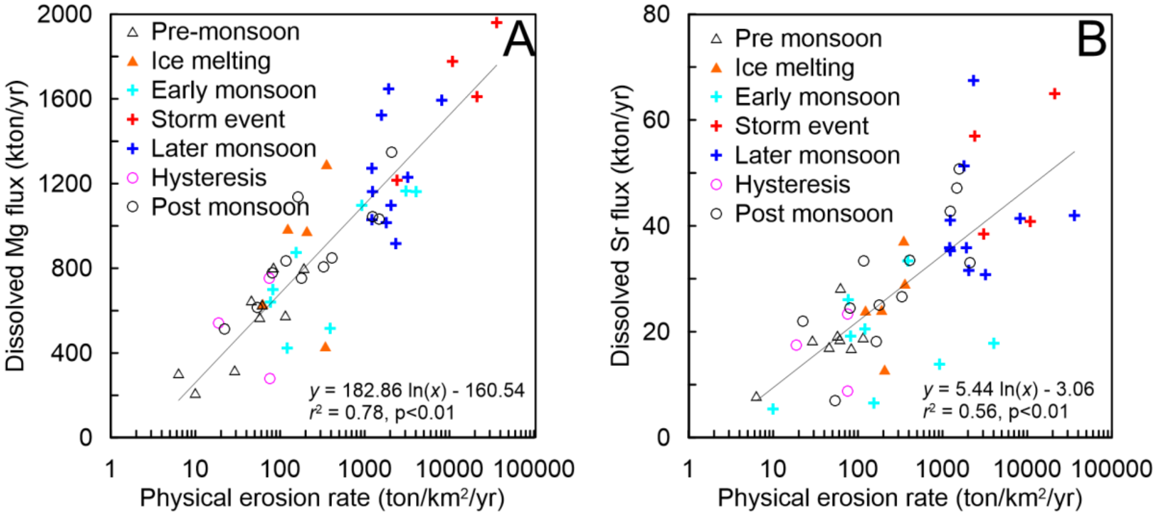

Figure 3 Exponential relationships of (A) dissolved Mg flux and (B) dissolved Sr flux with physical erosion rate (PER, from Zhang et al. (2015)) in the middle Yellow River, suggesting that chemical weathering is tightly related to physical erosion.

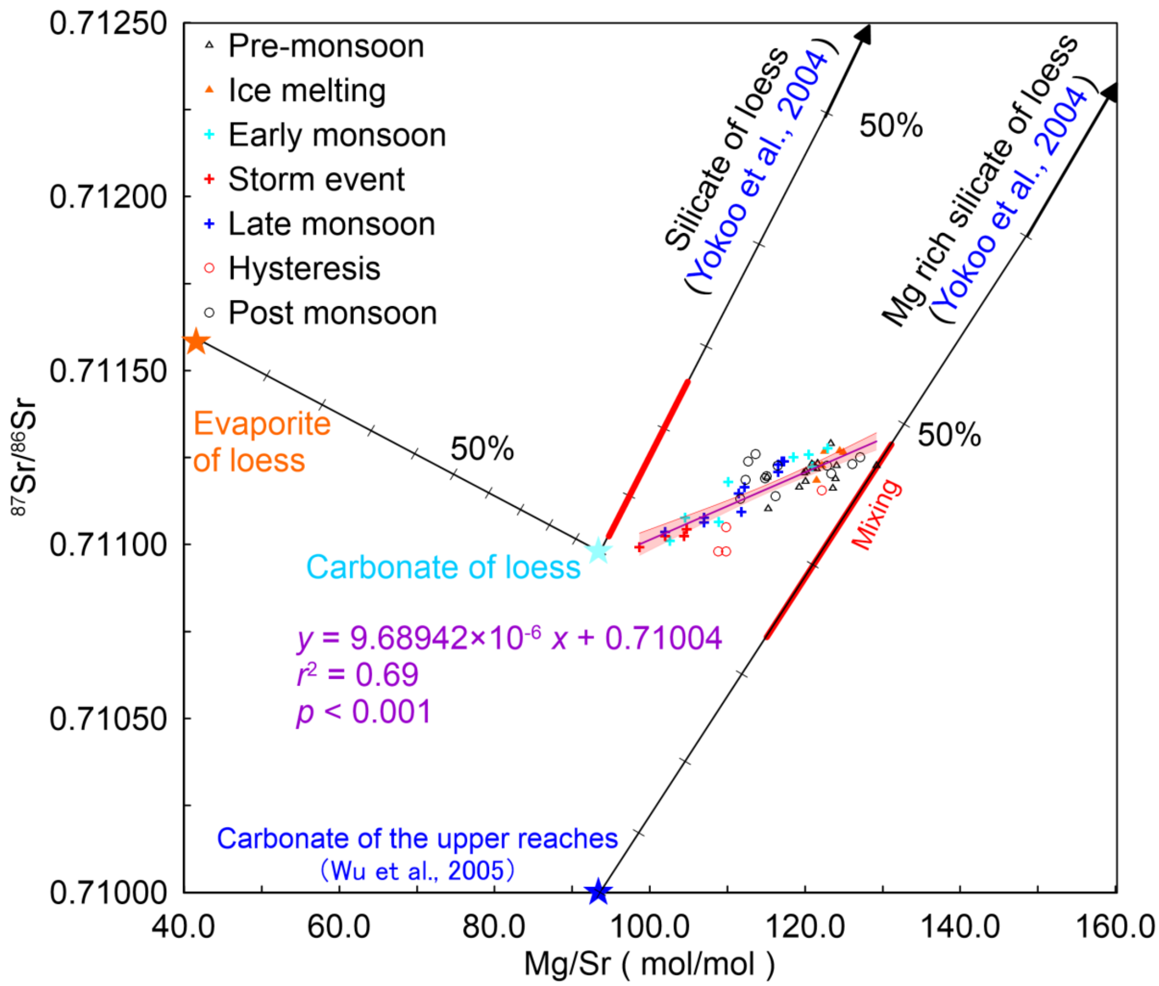

Figure 4 Mixing diagram of $^{87}Sr/^{86}Sr$ *vs*. Mg/Sr, showing that at the first order carbonate and silicate equally contribute to dissolved Sr isotopic compostions, but preferential removal of Mg relative to Sr is required to fully explain the seasonal data. The $^{87}Sr/^{86}Sr$ of three end members are 0.71158 ± 0.00112 for evaporite, 0.71953 ± 0.00498 for silicates, and 0.71098 ± 0.00082 for carbonates, as constrained by our own leaching experiments performed on loess samples. The $^{87}Sr/^{86}Sr$ composition of carbonate in the upper Yellow River is from Wu et al. (2005), while the composition of Mg-rich silicate (e.g., chlorite) is from Yokoo et al. (2004). The corresponding Mg/Sr ratios of the end-members are 41.6 ± 21.1 (evaporite); 93.3 ± 16.5 (carbonates); 290.7 ± 114.5 (silicates), and ~351.3 (Mg-rich silicates; as constrained from Yokoo et al. (2004). The Mg/Sr ratio of carbonates from the upper reaches is considered to

be the same as the one extracted from loess using HAc of our leaching experiments.

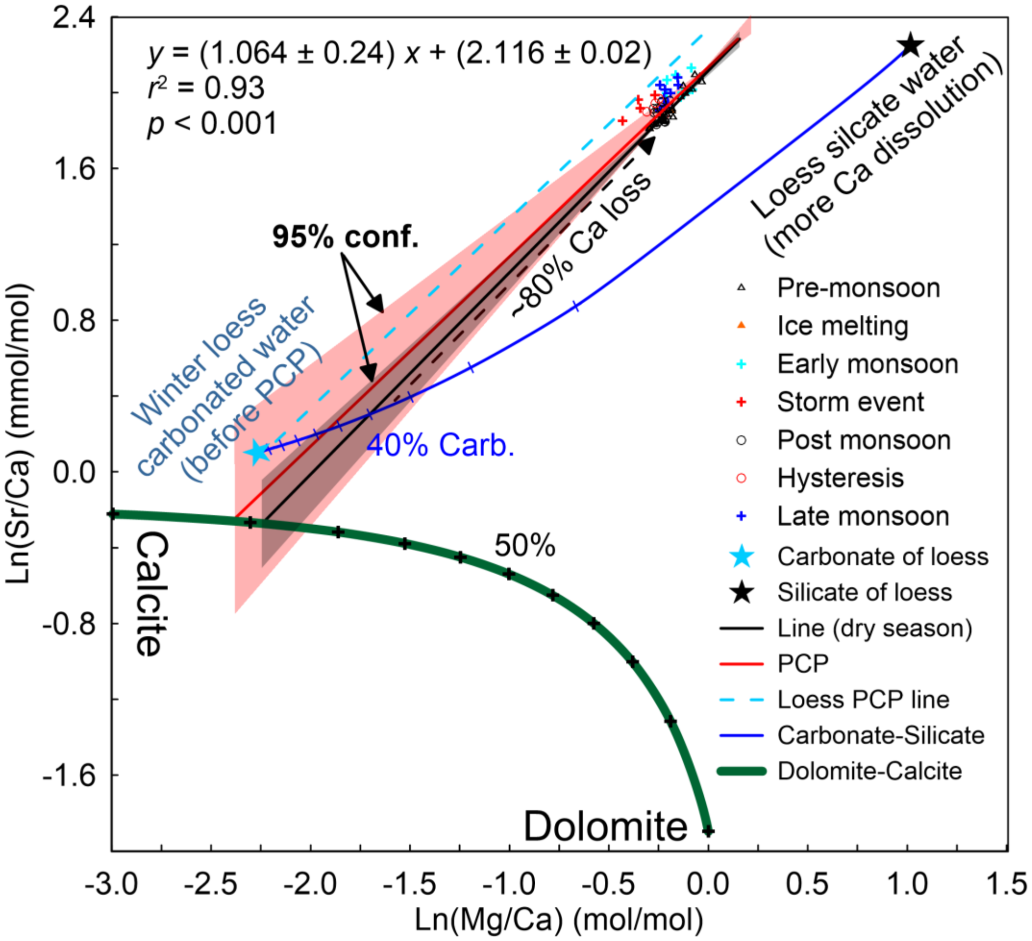

Figure 5 Plot of ln(Sr/Ca) *vs.* ln(Mg/Ca) to determine the effect of prior calcite precipitation (PCP) on Mg and Sr dissolved contents. Taking the entirety of our dataset into account, the relationship between two ratios is poor (r^2 = 0.47, red line) and its slope inconsistent with the PCP; in the dry season (LM13-1 to 25 and LM13-56 to 60), however, the slope is consistent with the PCP (0.85-1.45, r^2 = 0.93, black lines; Sinclair et al., 2012; Yang et al., 2015; Wassenburg et al., 2020). Variation in the riverine Mg/Sr ratios exactly lies between the mixing of the two PCP trends (each corresponding to dolomite and calcite as the end member, respectively). The mixing line between carbonate and silicate rocks (dark blue) intersects the PCP trend (black line) at 40 ± 11% carbonate contribution. Note that subtle variation in Mg/Sr of river waters is very likely a result of mixing between dissolved calcite and dolomite (Fig. 6).

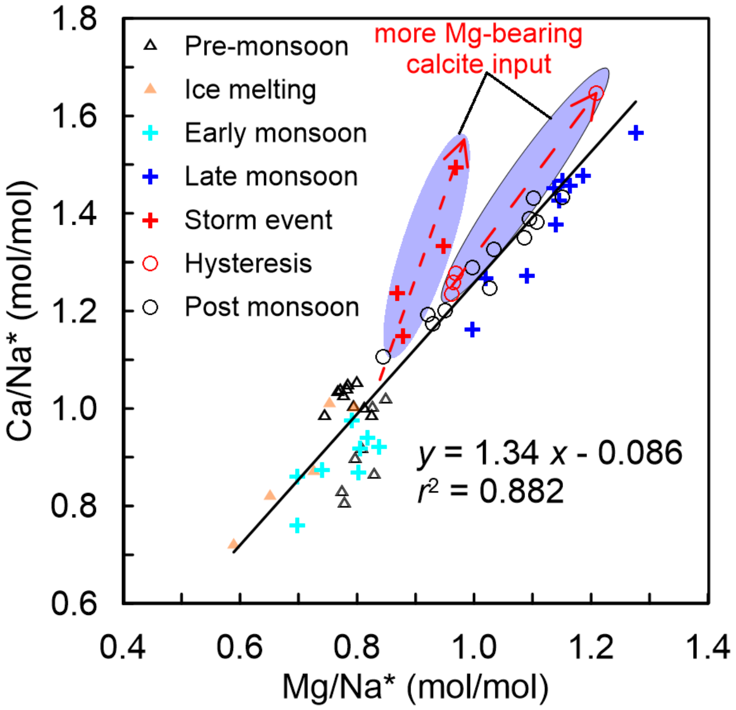

Figure 6 Ca/Na* against Mg/Na* ratios showing inputs of Mg from Mg-bearing carbonate during the storm event interval. Na* = Na^+ - Cl^- . Samples from the dry seasons that might have experienced the PCP have lower Ca/Na* due to Ca removal during carbonate precipitation (Fig. 5).

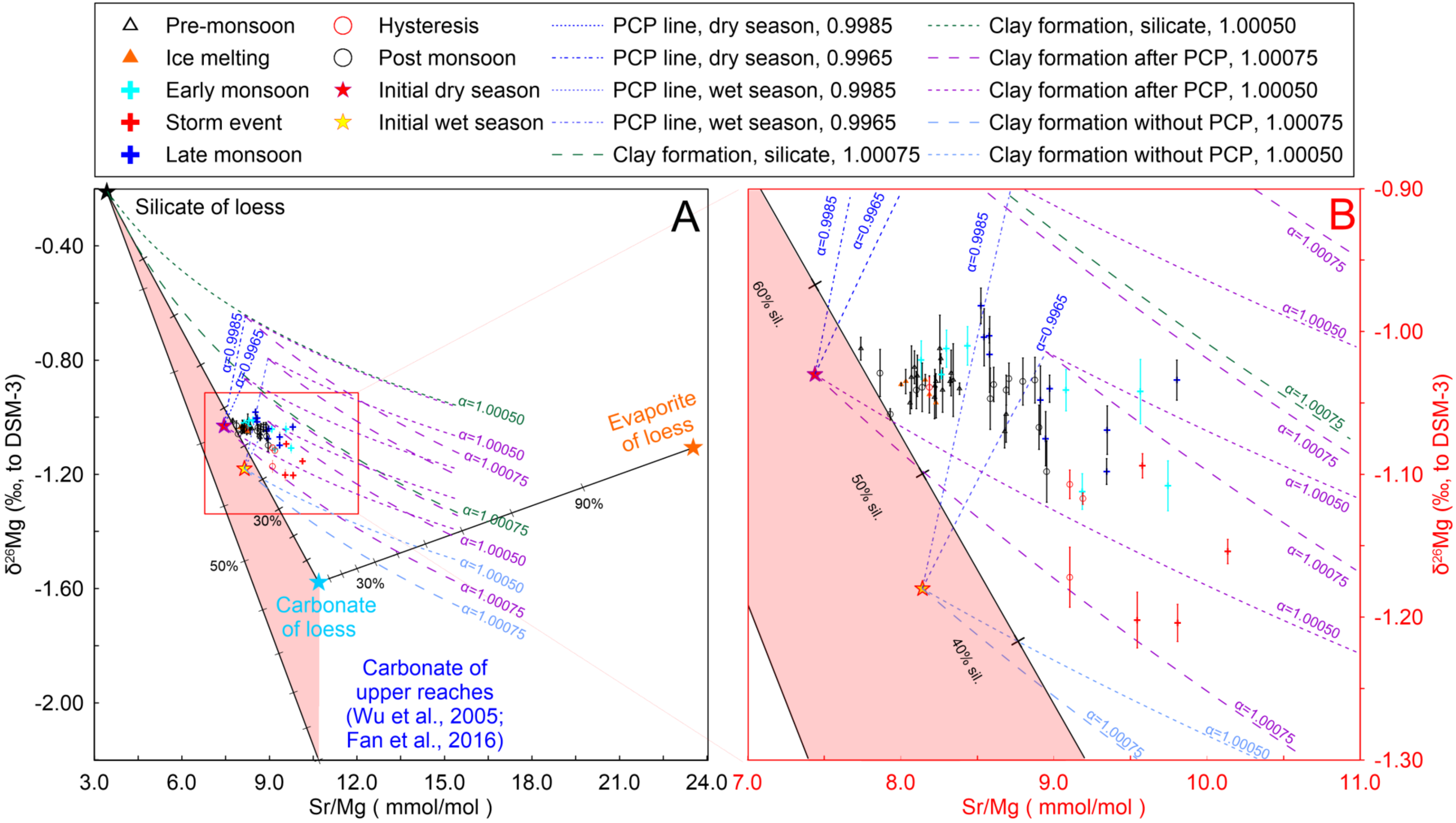
Pre-monsoon
Ice melting
Early monsoon
Storm event
Late monsoon
Hysteresis
Post monsoon
Initial dry season
Initial wet season
PCP line, dry season, 0.9985
PCP line, dry season, 0.9965
PCP line, wet season, 0.9985
PCP line, wet season, 0.9965
Clay formation, silicate, 1.00075
Clay formation, silicate, 1.00050
Clay formation after PCP, 1.00075
Clay formation after PCP, 1.00050
Clay formation without PCP, 1.00075
Clay formation without PCP, 1.00050
A
Silicate of loess
Evaporite of loess
Carbonate of loess
Carbonate of upper reaches (Wu et al., 2005; Fan et al., 2016)
α=0.9985
α=0.9965
α=1.00050
α=1.00075
30%
50%
90%
-0.40
-0.80
-1.20
-1.60
-2.00
δ26Mg (‰, to DSM-3)
3.0
6.0
9.0
12.0
15.0
18.0
21.0
24.0
Sr/Mg (mmol/mol)
B
60% sil.
50% sil.
40% sil.
-0.90
-1.00
-1.10
-1.20
-1.30
7.0
8.0
9.0
10.0
11.0

Figure 7 Rayleigh fractionation model for Mg isotopes simulatation during prior calcite precipitation (PCP) and clay formation. End members for Mg isotope compositions (i.e., evaporite, carbonate, and silicate in loess (Yokoo et al., 2004)), and carbonate of the upper Yellow River (Wu et al., 2005; Fan et al., 2016; Teng, 2017) are shown. ~32% of the TDS of the middle Yellow River is supplied by the upper Yellow River (with 40% *vs*. 60% for carbonate and silicate contributions; Li et al., 2018), and binary mixing of this TDS with loess-derived Mg in the middle Yellow River. The Mg isotope ratio before the PCP ($\delta^{26}Mg_{pre\text{-}PCP}$) value of -1.03‰ (using a Mg isotope composition of -0.22‰ for silicates and -2.2‰ for carbonates; Fan et al., 2016) and the Sr/Mg ratio is 7.44 in the dry seasons (red star). Similarly, in the wet seasons, the input of Mg-bearing calcite (Fig. 6) results in a decrease of $^{87}Sr/^{86}Sr$ of 0.0003 and $\delta^{26}Mg$ of 0.2‰, considering the Sr and Mg isotopic compositions of carbonates in the loess, corresponding to an elevated proportion of carbonate by about 10%. Therefore, the $\delta^{26}Mg_{pre\text{-}PCP}$ is estimated to be -1.18‰ and its Sr/Mg ratio is 8.14 in the wet seasons (yellow star). Experimental work suggests that the approximate fractionation factors for the PCP are between 0.9965 and 0.9985 depending on the precipitation rates (Mavromatis et al., 2013; Saenger et al., 2014), whereas the fractionation factors for clay formation are in the range 1.00050-1.00075 (Wimpenny et al., 2010). Because the PCP resultes ~80% Ca loss, and ~6% Mg loss (Fig. 5), we employ a D_{Mg} of 0.07 (Sinclair et al., 2012; Li and Li, 2013; Wassenburg et al., 2020) to calculate the Mg isotope shift of ~0.17‰ to 0.39‰.